Electronic Supplementary Information for

Mechanistic Investigation of the Nickel-Catalyzed Carbonylation of Alcohols

*Sara Sabater,[1,#] Maximilian Menche,[1,2,#] Tamal Ghosh,[1] Saskia Krieg,[3] Katharina S. L. Rück,[4] Rocco Paciello,[4] Ansgar Schäfer,[2] Peter Comba, [3] A. Stephen K. Hashmi[1,5] and Thomas Schaub[*1,4]*

[1]Catalysis Research Laboratory (CaRLa), Im Neuenheimer Feld 584, 69120 Heidelberg, Germany.

[2]BASF SE, Quantum Chemistry, Carl-Bosch-Straße 38, 67056 Ludwigshafen, Germany.

[3]Anorganisch-Chemisches Institut, Heidelberg University, Im Neuenheimer Feld 270, 69120 Heidelberg, Germany.

[4]BASF SE, Organic Synthesis, Carl-Bosch-Straße 38, 67056 Ludwigshafen, Germany.

[5]Organisch-Chemisches Institut, Heidelberg University, Im Neuenheimer Feld 270, 69120 Heidelberg, Germany.

Table of Contents

S1. Screening Experiments

Table S1. Screening of Ni salts for the carbonylation of 1-phenylethanol.[a]

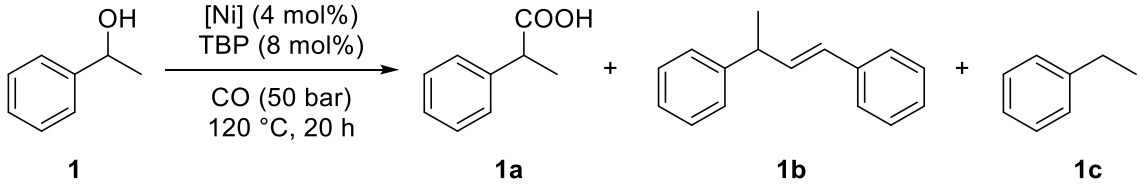

Entry	[Ni]	Yield 1a (%)[b]	Yield 1b (%)[b]	Yield 1c (%)[b]
1	--	0	0	0
2	NiI_2	83	11	4
3	$NiBr_2$	20	8	5
4	$NiCl_2$	8	1	1
5	$Ni(OAc)_2$	0	0	0
6	$Ni(OTf)_2$	0	14	11
7	$Ni(acac)_2$	0	0	0
8	Ni(2-ethylhexanoate)$_2$	0	0	0

[a] A mixture of 1-phenylethanol (8.3 mmol), [Ni] (4 mol%) and TBP (8 mol%) was pressurized with CO at 50 bar, and stirred at 120 °C for 20 h. [b] Yields were determined by GC-FID chromatography using anisole as an internal standard after derivatization with *N*-methyl-*N*-(trimethylsilyl) trifluoroacetamide.

Table S2. Evaluation of catalytic components.[a]

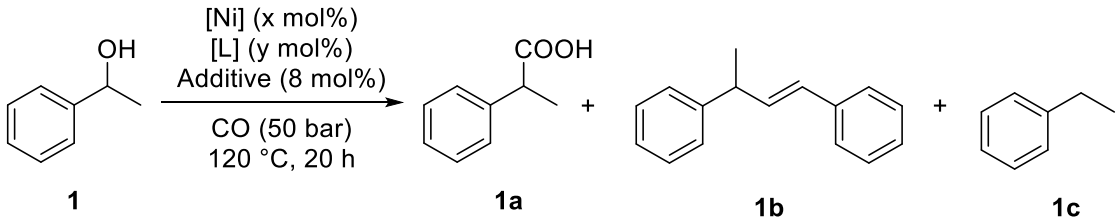

Entry	[Ni] (4 mol%)	[L] (8 mol%)	Additive	Yield 1a (%)[b]	Yield 1b (%)[b]	Yield 1c (%)[b]
1	NiI_2 (2 mol%)	TBP (4 mol%)	-	16	20	4
2[c]			H_2O	0	4	4
3			$Mo(CO)_6$	7	6	9

4		HAc[d]	3	28	40
5		HI[e]	0	50	15
6		MsOH	0	27	5
7		LiI	70	17	5
8		H_2[f]	15	6	10

[a] A mixture of 1-phenylethanol (8.3 mmol), [Ni] (2 or 4 mol%), TBP (4 or 8 mol%) and the corresponding additive (8 mol%) when indicated, was pressurized with CO at 50 bar, and stirred at 120 °C for 20 h. [b] Yields were determined by GC-FID chromatography using anisole as an internal standard after derivatization with *N*-methyl-*N*-(trimethylsilyl) trifluoroacetamide. [c] bis(1-phenylethyl)ether was obtained as the main product. [d] 6 M. [e] 57% in water. [f] CO, H_2 (5:1) mixture.

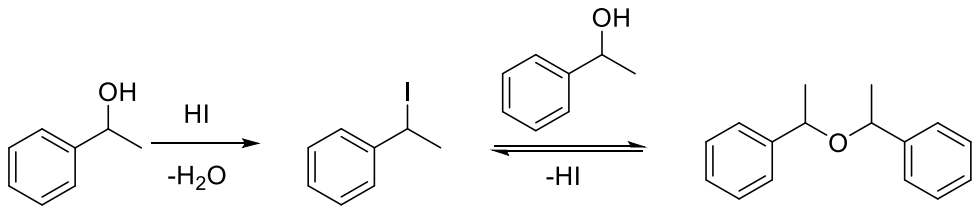

Scheme S1. Formation of bis-(1-phenylethyl)ether.

Table S3. Ligand screening (cont..).[a]

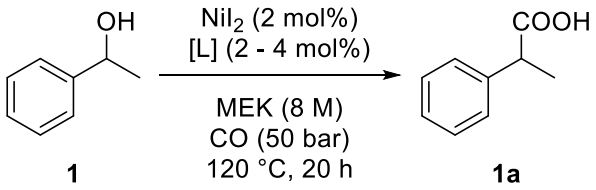

Entry	[L]	(mol%)	Yield 1a(%)[b]
1	Py	4	0
2	DMAP	4	0
3	8-Hyrdoxyquinoline	4	0
4	$P(OMe)_3$	4	0
5	$P(OPh)_3$	4	0
6	2,2'-Bipy	2	0
7	1,10-Phenantroline	2	5

[a] A mixture of 1-phenylethanol (8.3 mmol), NiI_2 (2 mol%), the corresponding ligand (2 or 4 mol%), in MEK (8 M) was pressurized with CO at 50 bar, and stirred at 120 °C for 20 h. [b] Yields were determined by GC-FID chromatography using anisole as an internal standard after derivatization with *N*-methyl-*N*-(trimethylsilyl) trifluoroacetamide.

Table S4. Variation LiI concentration.[a]

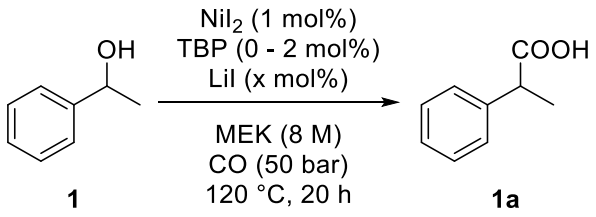

Entry	[LiI] (x mol%)	Yield 1a (%)[b] (0 mol% TBP; 1 mol% Hünig's base)	Yield 1a (%)[b] (0 mol% TBP; 2 mol% Hünig's base)
1	-	nd	Nd
2	2	14	4
3	4	20	4
4	8	49	8
5	20	52	18

[a] A mixture of 1-phenylethanol (8.3 mmol), NiI_2 (1 mol%), Hünig's base (1-2 mol%) when indicated and LiI (x mol%) was pressurized with CO at 50 bar, and stirred at 120 °C for 20 h. [b] Yields were determined by GC-FID chromatography using anisole as an internal standard after derivatization with *N*-methyl-*N*-(trimethylsilyl) trifluoroacetamide.

Table S5. Ligand screening using 20 mol% of LiI.[a]

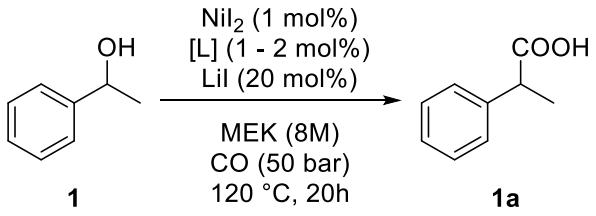

Entry	[L]	Yield 1a(%)[b]
1	TBP	63
2	PCy_3	64
3	PPh_3	58
4 [c]	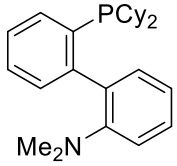	66

5 [c]	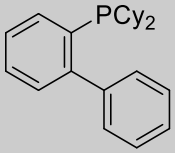	65
6 [c]	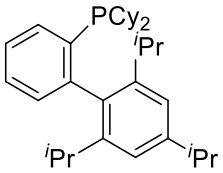	66
7 [c]	dCype	30
8 [c]	dppe	26
9 [c]	dppp	55
10 [c]	dppb	56
11 [c]	dpppe	50
12	Py	3
13	DMAP	2
14 [c]	2,2'-Bipy	2
15 [c]	1,10-Phenantroline	4

[a] A mixture of 1-phenylethanol (8.3 mmol), NiI_2 (1 mol%), the corresponding ligand (1 or 2 mol%) and LiI (20 mol%) in MEK (8 M) was pressurized with CO at 50 bar, and stirred at 120 °C for 20 h. [b] Yields were determined by GC-FID chromatography using anisole as an internal standard after derivatization with *N*-methyl-*N*-(trimethylsilyl) trifluoroacetamide. [c] 1 mol%.

Table S6. MX screening.[a]

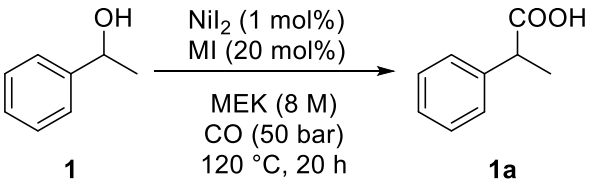

Entry	MI	Yield 1a (%)[b]
1	-	0
2	LiI	56
3[c]	LiI	0
4	NaI	66
5	Bu_4PI	39
6	Bu_4NI	4
7	NH_4I	3

[a] A mixture of 1-phenylethanol (8.3 mmol), NiI_2 (1 mol%) and the corresponding MI (20 mol%) in MEK (8 M) was pressurized with CO at 50 bar, and stirred at 120 °C for 20 h. [b] Yields were determined by GC-FID chromatography using anisole as an internal standard after derivatization with *N*-methyl-*N*-(trimethylsilyl) trifluoroacetamide. [c] Reaction run in the absence of NiI_2.

Table S7. Radical scavenger test studies.[a]

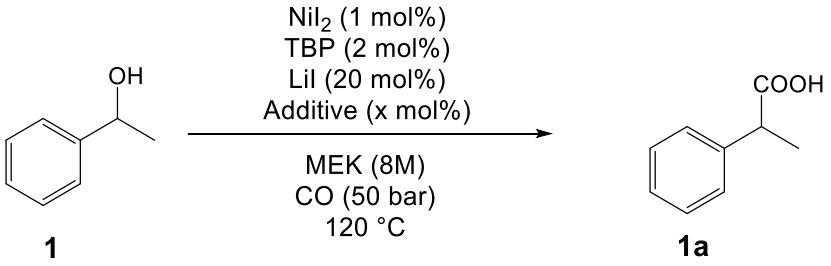

Entry	[Additive]	(mol%)	Yield 1a(%)[b]
1	-	-	63
2[c]	TEMPO	5	2
3	$FeCl_3$	5	44
4	^tBuONO	5	42
5	AIBN	5	65
6[c]	Bu_3SnH	5	0
7	Ascorbic Acid	5	58
8	IrgaPhos	5	43
9	Hydroquinone	5	52
10		25	24
11		100	5
12	2,6-di-t-butyl-4-methylphenol	5 25	53
13		100	59
14			55

[a] A mixture of 1-phenylethanol (8.3 mmol), NiI_2 (1 mol%), TBP (2 mol%), LiI (20 mol%) and the corresponding additive (5 mol%) when indicated, in MEK (8M) was pressurized with CO at 50 bar, and stirred at 120 °C for 20 h. [b] Yields were determined by GC-FID chromatography using anisole as an internal standard after derivatization with *N*-methyl-*N*-(trimethylsilyl) trifluoroacetamide. [c] Color changed when the additive was added.

Entry 11:

Observed: Main Product

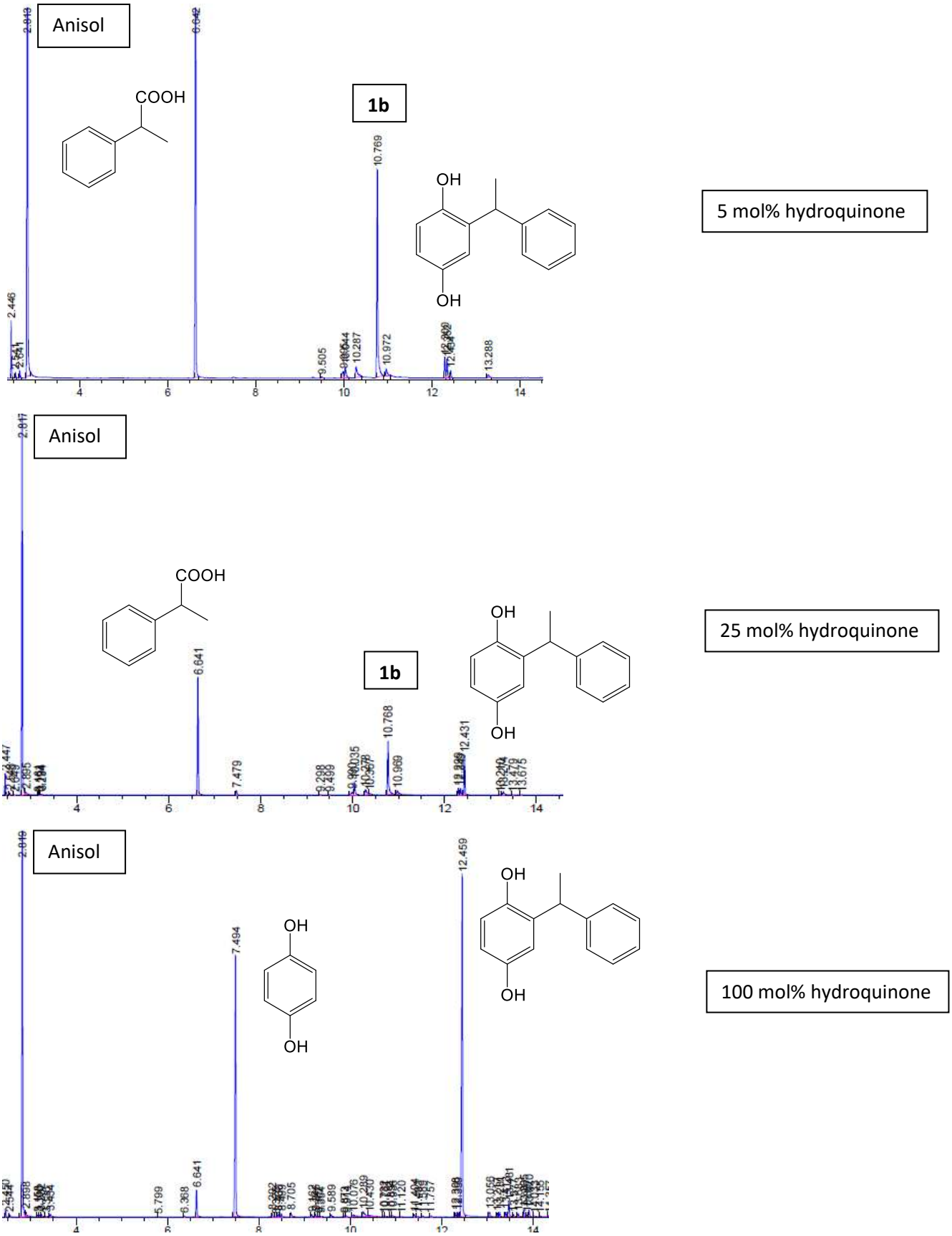

Figure S1. GC-FID chromatograms for entries 9 (top), 10 (middle) and 11 (bottom), showing a dependence of the concentration of hydroquinone and the formation of side product.

S2. General information

Unless otherwise noted, all reactions and manipulations were carried out under an Ar atmosphere using standard Schlenk and high-vacuum-line techniques or in a Braun inert-atmosphere glovebox (Ar) at ambient temperature. Organic solvents were purchased dry from Aldrich and degassed prior to use by bubbling argon for at least 30 min. Commercially available chemicals were purchased from Aldrich, ABCR, or TCI and were used as received unless otherwise stated. NMR spectra were recorded using a Bruker 200 instrument at CaRLa or Bruker AVANCE III 300, Bruker AVANCE III 400, Bruker AVANCE III 500 and Bruker AVANCE III 600 spectrometers at the Institute of Organic Chemistry of University of Heidelberg. ^{1}H and ^{13}C chemical shifts δ are reported in ppm relative to either the residual solvent or tetramethylsilane (TMS). ^{31}P chemical shifts are reported relative to an external standard of phosphoric acid 30% in D_2O (0.0 ppm). The multiplicities are reported as s = singlet, b = broad, d = doublet, t = triplet, q = quartet, sept = septet, and m = multiplet. GC analyses were performed on an Agilent Technologies 6890N gas chromatography system equipped with an FID detector and an Agilent Technologies DB-5, (5%-phenyl)methylpolysiloxane, capillary column (30 m × 0.320 mm × 0.25 μm; He flow 1.0 mL/min; program initial 80 °C, ramp 15 °C/min, 300 °C for 5 min). GC-MS analyses were performed on an Agilent Technologies 6890N gas chromatography system coupled with an Agilent Technologies 5975B mass spectrometer and equipped with an Agilent Technologies HP-5MS capillary column (30 m × 0.250 mm/ 0.25 μm). Elemental analysis were conducted in house. X-Band EPR spectra were recorded on a Bruker Elexsys E500 instrument equipped with a ER 4112HV-CF58nc In-Cavity Cryogen Free VT System in perpendicular mode at 9.63 GHZ at 203 K.

Caution*: Caution: Carbon Monoxide (CO) is an extremely poisonous substance. Proper safety precautions need to be applied and appropriate safety equipment MUST be used. Reactions must be carried out in a well-ventilated fume hood equipped with a CO detector. The CO bottle*

was stored outside the laboratory and was permanently connected to a gas distribution system equipped with magnetic safety valves. The valves were connected to CO sensors inside the laboratory. Additionally, all the reactions involving the use of CO were carried out using a portable CO detector and personal protection equipment.

S3. Synthesis and characterization data

S3.1. TBP·HI

Synthesis of TBP·HI: In a Schlenk flask, a 57% aqueous solution of HI (1.3 mL, 9.8 mmol) was added dropwise to TBP (2 mL, 8 mmol) under Argon, at room temperature. The mixture was stirred for 18 h and then extracted using dichloromethane/water mixtures. The organic layers were combined and the solvent was removed under reduced pressure to afford a white solid. Yield: 2,3 g, 87%. ^{1}H NMR (600 MHz, C_6D_6): δ 7.66 (dsept, $^{1}J_{PH}$ = 490 Hz, $^{3}J_{HH}$ = 5.6 Hz, 1H), 2.57 – 2.47 (m, 6H, P-C*H*$_2$-), 1.57 – 1.48 (m, 6H, -C*H*$_2$-), 1.43 – 1.33 (m, 6H, -C*H*$_2$-), 0.91 (t, J = 7.3 Hz, 9H, -C*H*$_3$). ^{13}C{^{1}H} NMR (151 MHz, C_6D_6): δ 25.1 (d, J = 4.7 Hz), 24.1 (d, J = 15.5 Hz), 17.6 (d, J = 46.8 Hz), 13.8 (s). ^{31}P {^{1}H} NMR (243 MHz, C_6D_6): δ 8.83 (s). Anal. Calcd. For $C_{12}H_{28}PI$ (330.10 g/mol): C, 43.65; H, 8.55. Found: C, 43.68; H, 8.70.

NMR spectra of TBP·HI:

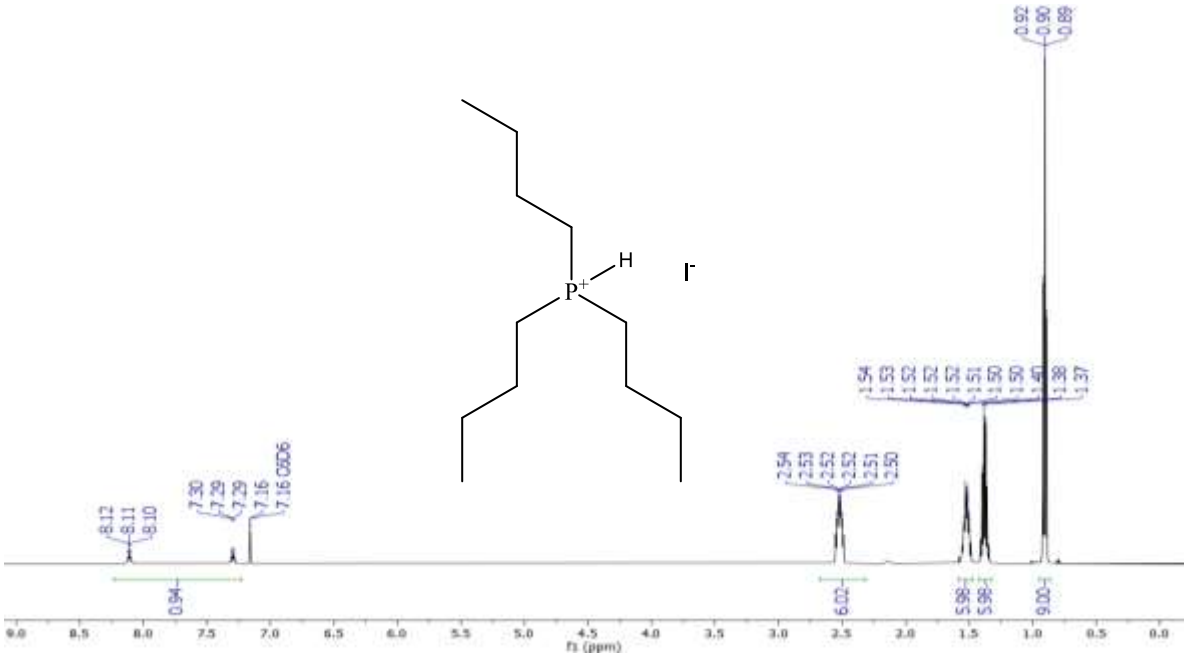

Figure S2. ^{1}H NMR spectrum of TBP·HI (600 MHz, C_6D_6, 298K)

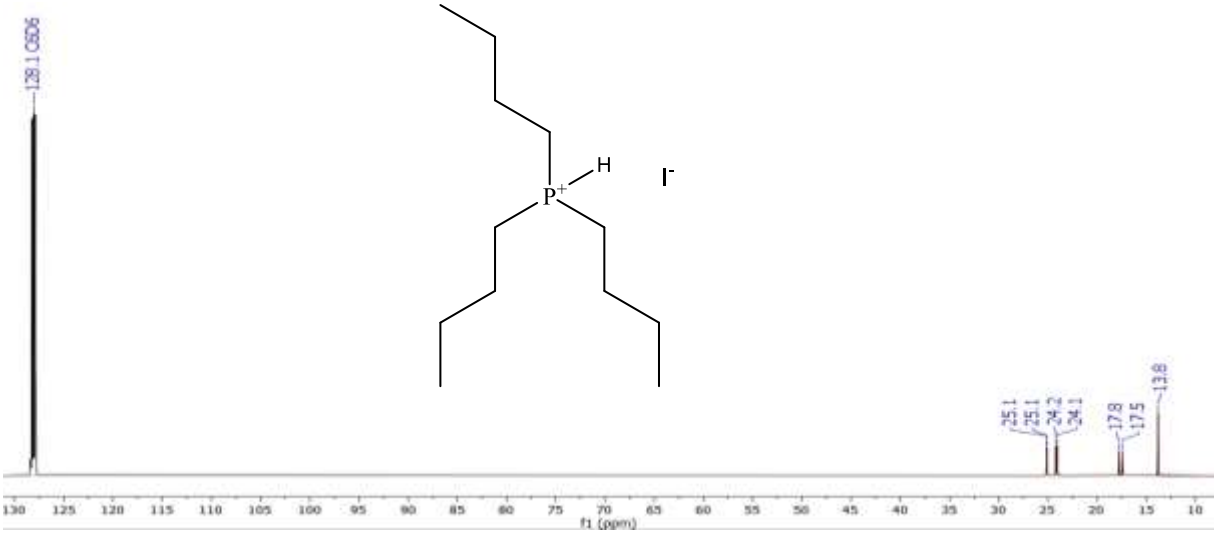

Figure S3. $^{13}C\{^{1}H\}$ NMR spectrum of TBP·HI (151 MHz, C_6D_6, 298K)

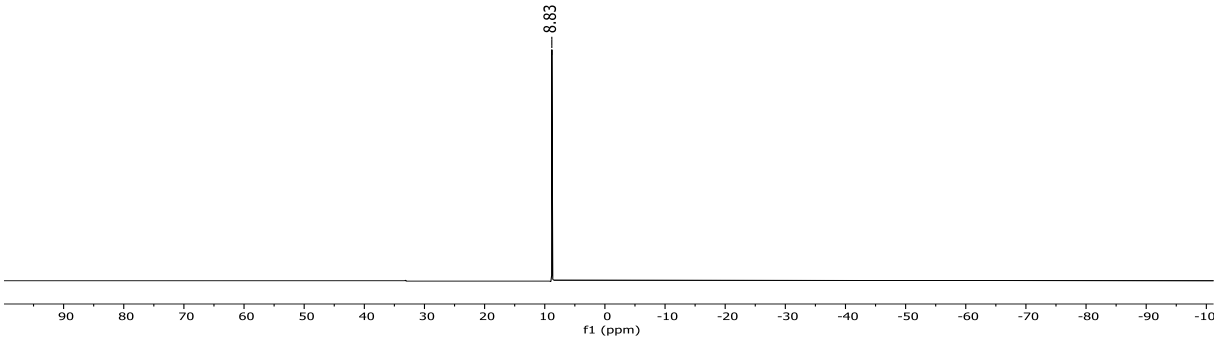

Figure S4. ^{31}P $\{^{1}H\}$ NMR spectrum of TBP·HI (243 MHz, C_6D_6, 298K)

S3.2. EPR simulation

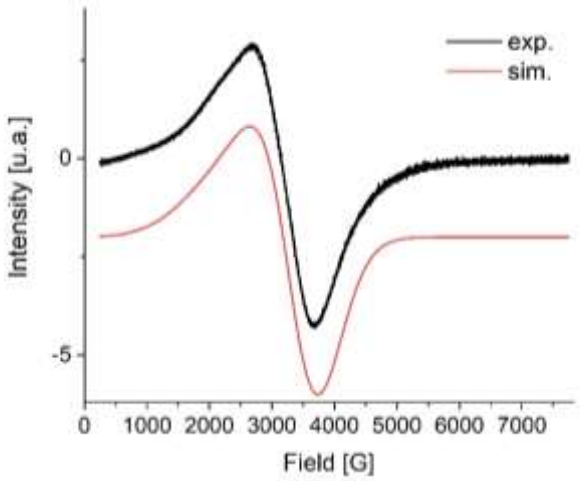

Figure S5. Black: X-band (9.638417 GHz) EPR spectrum at 203 K of the reaction mixture of $Ni(PPh_3)_2(CO)_2$ and iodocyclohexane in methyl ethyl ketone at 90 °C. Red: Simulated EPR spectrum. The Simulation was carried out with the XSophe Computer Simulation Software

Suite (Version 1.1.4) using following parameters: $g_x = g_y = 2.05$; $g_z = 2.95$; linewidth x = linewidth y = 505 G, linewidth z = 825 G for a Ni(I) nucleus with S =1/2.

S4. Catalytic experiments

S4.1. Pictures of the autoclaves used

Two types of autoclaves were used for the experiments: a HEL CAT7 autoclave (volume: 7 x 10 mL, internal stirring bar 500 rpm, material: glass (vials) and stainless steel), and self-made Swagelok autoclaves (volume 15 mL, internal stirring bar 500 rpm, material: Teflon (insert) and stainless steel).

HEL CAT7 autoclave:

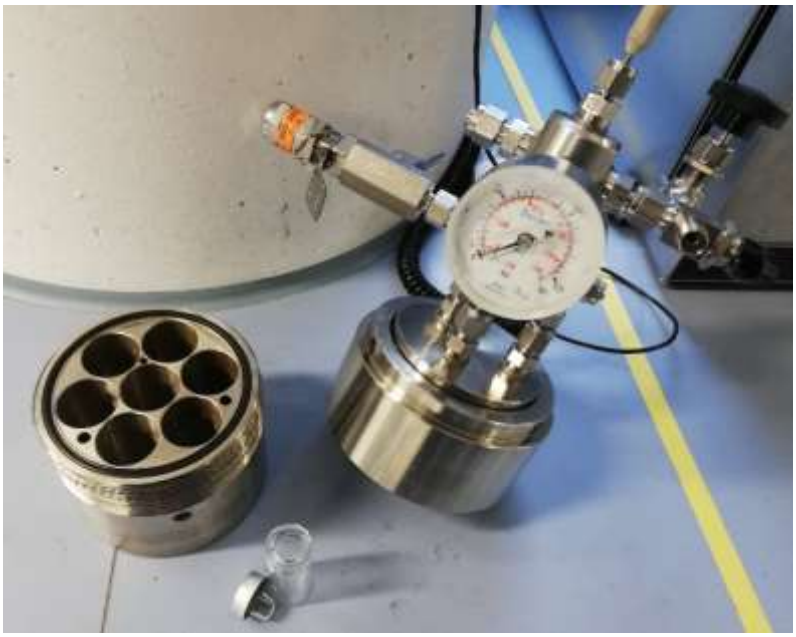

Self-made Swagelok autoclaves:

S4.2. Typical procedure for the carbonylation of 1-phenylethanol (HEL CAT7 screening experiments)

The corresponding nickel source, ligand and/or additive were placed in a 10 mL microwave glass vial under Ar atmosphere (Glovebox). 1-Phenylethanol (8.28 mmol) and methyl ethyl ketone (8 M) were added and the vials were closed with a septum cap fitted with a needle. The vials were placed in a HEL CAT7 autoclave which was flushed with carbon monoxide (3 x 5 bar) and then pressurized with carbon monoxide to 50 atm and heated to 120 °C for 20 h. The autoclave was cooled down to room temperature and the remaining pressure released in a well-ventilated hood. The crude mixtures were diluted with DCM (2 mL). *N*-Methyl-*N*-(trimethylsilyl) trifluoroacetamide (0.2 mL), DCM (1.5 mL), and the reaction mixture (0.1 mL) were added to a GC vial. The vial was heated on a steel plate to 70 °C for 1 h. The yield and selectivity were determined by GC-FID analysis using anisole as internal standard.

S4.3. Typical procedure for the carbonylation of benzylic alcohols (Procedure A)

A 15 mL self-made stainless steel autoclave from Swagelok parts fitted with a Teflon insert and a magnetic stirring bar was charged under Ar atmosphere with: NiI_2 (4 mol%), TBP (8 mol%), LiI (20 mol%), the corresponding alcohol (8.28 mmol) and methyl ethyl ketone (8 M). The autoclave was flushed with carbon monoxide (3 x 5 bar) and then pressurized with carbon

monoxide to 50 atm and heated to 120 °C in an oil bath for 20 h. The autoclave was cooled down to room temperature and the remaining pressure released in a well-ventilated hood. Isolated products were obtained by flash chromatography (Biotage Isolera Prime) using petroleum ether-ethyl acetate mixtures. Products were identified according to spectroscopic data of the commercially available compounds.

S4.4. Typical procedure for the carbonylation of aliphatic alcohols (Procedure B)

A 15 mL self-made stainless steel autoclave from Swagelok parts fitted with a Teflon insert and a magnetic stirring bar was charged under Ar atmosphere (glovebox) with: NiI_2 (4 mol%), TBP (8 mol%), LiI (20 mol%), the corresponding alcohol (8.28 mmol) and methyl ethyl ketone (8 M). Outside the glovebox, the corresponding equivalents, if needed, of degassed water were added. The autoclave was flushed with carbon monoxide (3 x 5 bar) and then pressurized with carbon monoxide to 50 atm and heated to 200 °C in an oil bath for 20 h. The autoclave was cooled down to room temperature and the remaining pressure released in a well ventilated hood. Isolated products were obtained by flash chromatography (Biotage Isolera Prime) using petroleum ether-ethyl acetate mixtures. Products were identified according to spectroscopic data of the commercially available compounds.

S5. Computational investigations

S5.1 Computational details

All geometry optimizations were carried out at the BP86/def2-SV(P)[1] level of theory with relativisticly corrected effective core potentials[2] (ECP) for iodine. Stationary points were verified via analysis of the vibrational frequencies at the level of geometry optimization. Final electronic energies were obtained by single-point calculations at the PBE0-D3(BJ)/def2-QZVPP[3] level of theory employing Grimme's D3 dispersion correction[4] incorporating Becke-Johnson damping.[5] All quantum-chemical calculations were carried out using the TURBOMOLE program[6] (Version 7.3) with the resolution-of-identity (RI) approximation[7] and the corresponding auxiliary basis sets[8] implemented in the program. Zero-point vibrational energies and thermodynamic corrections were obtained at the level of geometry optimization and scaled to the given reaction temperatures (120 °C). For all species, the thermodynamic

[1] (a) Perdew, J. P., Density-functional approximation for the correlation energy of the inhomogeneous electron gas. *Phys. Rev. B* **1986,** *33*, 8822-8824; (b) Becke, A. D., Density-functional exchange-energy approximation with correct asymptotic behavior. *Phys. Rev. A* **1988,** *38*, 3098-3100; (c) Weigend, F.; Ahlrichs, R., Balanced basis sets of split valence, triple zeta valence and quadruple zeta valence quality for H to Rn: Design and assessment of accuracy. *Phys. Chem. Chem. Phys.* **2005,** *7*, 3297-3305.

[2] Andrae, D.; Häußermann, U.; Dolg, M.; Stoll, H.; Preuß, H., Energy-adjusted ab initio pseudopotentials for the second and third row transition elements. *Theor. Chim. Acta* **1990,** *77*, 123-141.

[3] Ernzerhof, M.; Scuseria, G. E., Assessment of the Perdew–Burke–Ernzerhof exchange-correlation functional. *J. Chem. Phys.* **1999,** *110*, 5029-5036; (b) Weigend, F.; Furche, F.; Ahlrichs, R., Gaussian basis sets of quadruple zeta valence quality for atoms H–Kr. *J. Chem. Phys.* **2003,** *119*, 12753-12762; (c) Weigend, F.; Ahlrichs, R., Balanced basis sets of split valence, triple zeta valence and quadruple zeta valence quality for H to Rn: Design and assessment of accuracy. *Phys. Chem. Chem. Phys.* **2005,** *7*, 3297-3305.

[4] Grimme, S.; Antony, J.; Ehrlich, S.; Krieg, H., A consistent and accurate ab initio parametrization of density functional dispersion correction (DFT-D) for the 94 elements H-Pu. *J. Chem. Phys.* **2010,** *132*, 154104-154119.

[5] Grimme, S.; Ehrlich, S.; Goerigk, L., Effect of the damping function in dispersion corrected density functional theory. *J. Comput. Chem.* **2011,** *32*, 1456-1465.

[6] (a) Ahlrichs, R.; Bär, M.; Häser, M.; Horn, H.; Kölmel, C., Electronic structure calculations on workstation computers: The program system turbomole. *Chem. Phys. Lett.* **1989,** *162*, 165-169; (b) *TURBOMOLE V7.3 2018, a development of University of Karlsruhe and Forschungszentrum Karlsruhe GmbH*, TURBOMOLE GmbH, available from http://www.turbomole.com; (c) Treutler, O.; Ahlrichs, R., Efficient molecular numerical integration schemes. *J. Chem. Phys.* **1995,** *102*, 346-354.

[7] (a) Weigend, F., Accurate Coulomb-fitting basis sets for H to Rn. *Phys. Chem. Chem. Phys.* **2006,** *8*, 1057-1065; (b) Vahtras, O.; Almlöf, J.; Feyereisen, M. W., Integral approximations for LCAO-SCF calculations. *Chem. Phys. Lett.* **1993,** *213*, 514-518; (c) Eichkorn, K.; Treutler, O.; Öhm, H.; Häser, M.; Ahlrichs, R., Auxiliary basis sets to approximate Coulomb potentials. *Chem. Phys. Lett.* **1995,** *240*, 283-290; (d) Deglmann, P.; May, K.; Furche, F.; Ahlrichs, R., Nuclear second analytical derivative calculations using auxiliary basis set expansions. *Chem. Phys. Lett.* **2004,** *384*, 103-107.

[8] (a) Weigend, F.; Häser, M.; Patzelt, H.; Ahlrichs, R., RI-MP2: optimized auxiliary basis sets and demonstration of efficiency. *Chem. Phys. Lett.* **1998,** *294*, 143-152; (b) Hellweg, A.; Hättig, C.; Höfener, S.; Klopper, W., Optimized accurate auxiliary basis sets for RI-MP2 and RI-CC2 calculations for the atoms Rb to Rn. *Theor. Chem. Acc.* **2007,** *117*, 587-597.

reference concentration was set to $p = 0.01$, except for CO ($x = 50$ bar). Solvent corrections to Gibbs free energies in 1-phenylethanol were calculated for all species, except CO and CO_2, with the conductor-like screen model for real solvents (COSMO-RS)[9] carried out with the COSMOtherm program[10] (Version 18.0.0; Revision 4360; Parameters BP_TZVP_18.ctd). All energies discussed are Gibbs free energies (G) in kJ mol^{-1}. Connectivities between minima and transition states implied in figures and schemes were validated by intrinsic-reaction-coordinate (IRC) following calculations.[11] Pictures of molecular structures were generated with the CYLview[12] program.

A multitude of geometrical isomers were analysed for all complexes. Due to the vast number of structures, we have decided to limit the herein reported structures to the one lowest in energy for each species. Our attempts to locate transitions states for the homolytic cleavage of R-I or the radical recombination of the metal-centered radicals and R• were unsuccessful. Neither closed-shell nor open-shell methods (broken symmetry) nor potential energy surface scans revealed any significant barrier. We therefore propose these steps to be of barrierless nature, however, we cannot exclude that this is an artefact of the single-reference methods.

[9] (a) Klamt, A., Conductor-like Screening Model for Real Solvents: A New Approach to the Quantitative Calculation of Solvation Phenomena. *J. Phys. Chem.* **1995,** *99*, 2224-2235; (b) Klamt, A.; Jonas, V.; Bürger, T.; Lohrenz, J. C. W., Refinement and Parametrization of COSMO-RS. *J. Phys. Chem. A* **1998,** *102*, 5074-5085.
[10] (a) *COSMOtherm Version 18.0.0 (Revision 4360)*, COSMOlogic GmbH & Co KG, available from http://www.cosmologic.de; (b) Eckert, F.; Klamt, A., Fast solvent screening via quantum chemistry: COSMO-RS approach. *AIChE J.* **2002,** *48*, 369-385.
[11] Fukui, K., The path of chemical reactions - the IRC approach. *Acc. Chem. Res.* **1981,** *14*, 363-368.
[12] Legault, C. Y. *Cylview 1.0b*, Université de Sherbrooke, available from http://www.cylview.org, 2009.

S5.2. Initial thermodynamic considerations

As the exact structure of the catalytic system could not be determined experimentally, the stabilities of various potential key intermediates were investigated (see Scheme S2). Based on these results, the involvement of biscoordinated species was ruled out in all further pathways ($Ni(CO)_2$ (**S1**): ΔG^{393} = 197.5 kJ mol^{-1}; Ni(CO)(TBP) (**S2**): ΔG^{393} = 208.8 kJ mol^{-1}; $Ni(TBP)_2$ (**S3**): ΔG^{393} = 284.9 kJ mol^{-1}). The tricoordinated complexes $Ni(CO)_2$(TBP) (**S5**) and $Ni(CO)(TBP)_2$ (**S4**) are significantly more stable. **S5** in which Ni is coordinated to one TBP ligand and two CO fragments (ΔG^{393} = 97.0 kJ mol^{-1}) is more stable than the other tricoordinated complex **S4** which incorporates two phosphine moieties (ΔG^{393} = 136.9 kJ mol^{-1}). This might be attributed to steric clash of the two large phosphine ligands. $Ni(CO)_3$ is similarly stable to phosphine mono-substituted **S5** (ΔG^{393} = 97.9 kJ mol^{-1}).

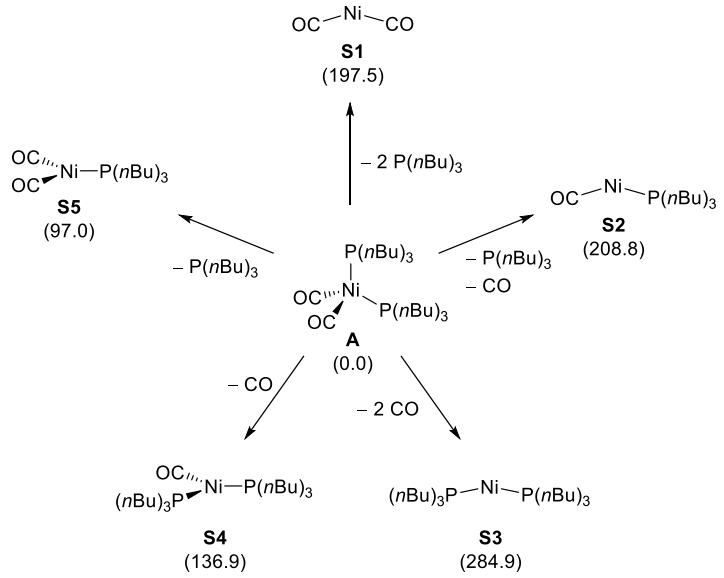

Scheme S2. Thermodynamic stabilities of potential biscoordinated and tricoordinated key intermediates in the Ni-catalyzed carbonylation of alkyl- and benzyliodides. ΔG^{393} in kJ mol^{-1}; RI-PBE0-D3(BJ)/def2-QZVPP//BP86/def2-SV(P); COSMO-RS (1-phenylethanol).

Secondly, to evaluate in which fashion the Ni center is substituted, all tetracoordinated isomers were investigated (Scheme S3). This enabled us to draw the following conclusions that were taken into account in all subsequently calculated mechanistic pathways: (1) **A** (ΔG^{393} =

0.0 kJ mol^{-1}) and **S7** (ΔG^{393} = 0.2 kJ mol^{-1}) are equal in energy and represent the most stable of the investigated structures. Both complexes will be present in equilibrium and are parallel starting points for our mechanistic investigations. (2) Ni(CO)$_4$ (**K**; ΔG^{393} = 42.0 kJ mol^{-1}) is significantly less stable than the mono- and bissubstituted TBP complexes (**A** and **S7**) and will not act as a resting state for the catalytic system. (3) The two complexes with three and four TBP ligands are the two least stable structures: **S6** (ΔG^{393} = 68.0 kJ mol^{-1}) and **S8** (ΔG^{393} = 153.3 kJ mol^{-1}).

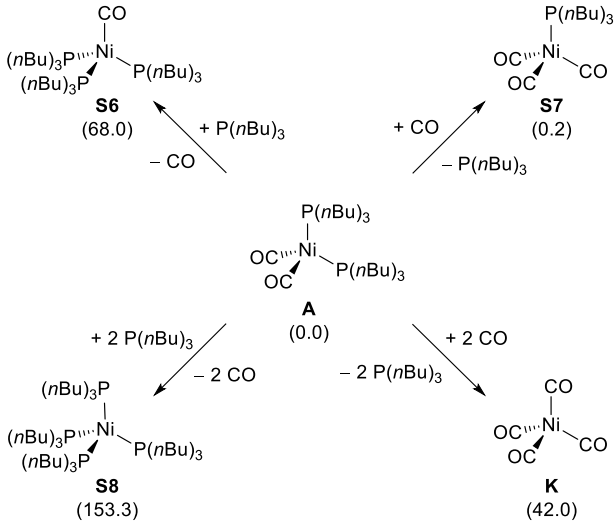

Scheme S3. Thermodynamic stabilities of possible tetracoordinated Ni-carbonyl-TBP compounds. ΔG^{393} in kJ mol^{-1}; RI-PBE0-D3(BJ)/def2-QZVPP//BP86/def2-SV(P); COSMO-RS (1-phenylethanol).

S5.3. Reaction pathway with two phosphines and one CO ligand coordinated to Ni

As two equivalents of phosphine have been shown to significantly improve reaction outcome, a possible mechanistic scenario that requires two coordinated phosphine ligands was probed (see Scheme S4).

The reaction proceeds in a similar fashion to the reaction with one phosphine ligand (TBP) coordinated to Ni (cf. Scheme 6). A detailed description of the mechanistic pathway is given in the manuscript. The activation barrier for the carbonylation with the complex with two

phosphine moieties is significantly higher than for the previously presented mechanism with one TBP ligand which is presented in Scheme 6 ($\Delta\Delta G^{\ddagger}$ = 38.4 kJ mol^{-1}). Furthermore, the reaction barrier of the phosphine biscoordinated system would be too high to be feasible for the given reaction conditions ($\Delta G^{\ddagger}$ = 152.4 kJ mol^{-1}).

Therefore, the suggested reaction mechanism will only incorporate one TBP coordinated to the metal center, while the other equivalent of phosphine is most likely assisting reaction steps that could not be probed computationally. This was later supported by experiments incorporating one equivalent of phosphine and Hünig's base (see manuscript).

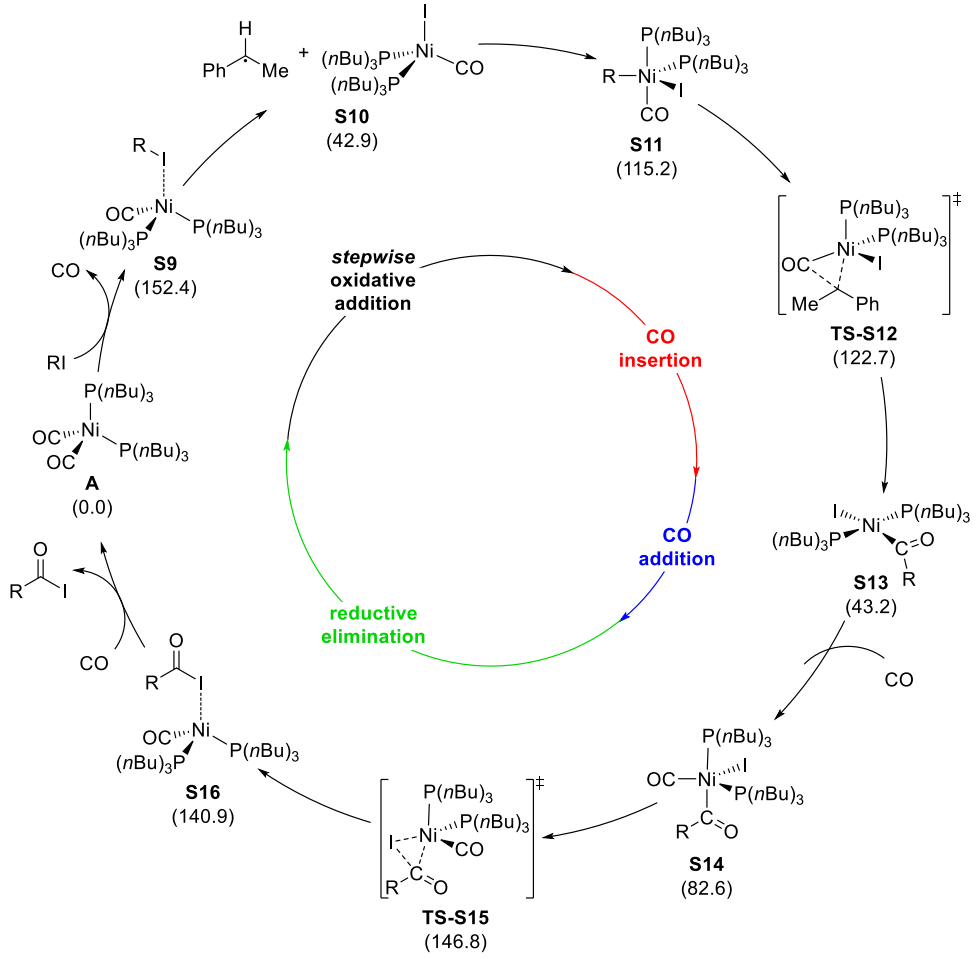

Scheme S4. Catalytic cycle for the carbonylation of RI via 'stepwise' oxidative addition via the Ni(I) complex coordinated to two phosphines and one CO ligand. ΔG^{393} in kJ mol^{-1}; RI-PBE0-D3(BJ)/def2-QZVPP//BP86/def2-SV(P); COSMO-RS (1-phenylethanol).

Secondly, 'classical' two-electron oxidative addition transition states were attempted to be calculated (Scheme S5). However, localization of the oxidative addition transition state was not successful. We attribute these problems to a highly unstable nature of this transition state, which could be further influenced by steric repulsion of the two bulky phosphine ligands. A reaction via Ni(I) (Scheme S4) will be preferred and the coordination of only one phosphine ligand was computed to be significantly more favourable (see Scheme 6 in the manuscript).

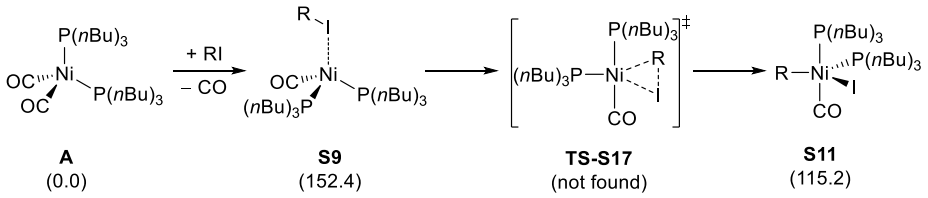

Scheme S5. Reaction pathway for the carbonylation of RI via two-electron oxidative addition via the Ni complex coordinated by two phosphines and one CO ligand. ΔG^{393} in kJ mol^{-1}; RI-PBE0-D3(BJ)/def2-QZVPP//BP86/def2-SV(P); COSMO-RS (1-phenylethanol).

S5.4. Reaction pathway with three CO ligands coordinated to Ni

Due to the equilibrium of $Ni(CO)_2(TBP)_2$ (**A**) and $Ni(CO)_3(TBP)$ (**S7**) not only the previously described pathways with one or two TBP ligands coordinated to the metal center are accessible (vide supra), but also a reaction pathway in which no phosphine is coordinating to nickel. This mechanistic scenario can be accessed by dissociation of TBP from $Ni(CO)_3(TBP)$ (**S7**) to form tricoordinated species $Ni(CO)_3$ which is further reacting with RI to form the corresponding adduct complex **S18**. On the other hand, $Ni(CO)_3$ and the subsequent alkylhalide adduct **S18** could form when no phosphine is used in the reaction. In this case, $Ni(CO)_4$ is formed, which might undergo CO dissociation to $Ni(CO)_3$ (see Scheme S6). In the following, only the calculated reaction mechanism starting from $Ni(CO)_4$ is reported as $Ni(CO)_4$ exhibits a higher relative energy and will therefore lead to lower reaction barriers for the phosphine-free mechanistic pathway. Based on our initial thermodynamic considerations, the relative energies of all intermediates and transitions states relative to the TBP coordinated complexes will be

significantly higher for the $Ni(CO)_2(TBP)_2$ (**A**) and $Ni(CO)_3(TBP)$ (**S7**) complexes ($\Delta\Delta G^{393}$ = 42.0 kJ mol^{-1} and $\Delta\Delta G^{393}$ = 41.8 kJ mol^{-1}, respectively; cf. Scheme S3). The reaction starting from $Ni(CO)_4$ proceeds in a similar fashion to the ones with phosphine coordinated to Ni (cf. Scheme 6 and Scheme S4). A detailed description of the mechanistic pathway is given in the manuscript. The activation barrier for the carbonylation with the complex with two phosphine moieties is significantly higher than for the previously presented mechanism with one TBP ligand which is presented in Scheme 6 ($\Delta\Delta G^{‡}$ = 14.3 kJ mol^{-1}).

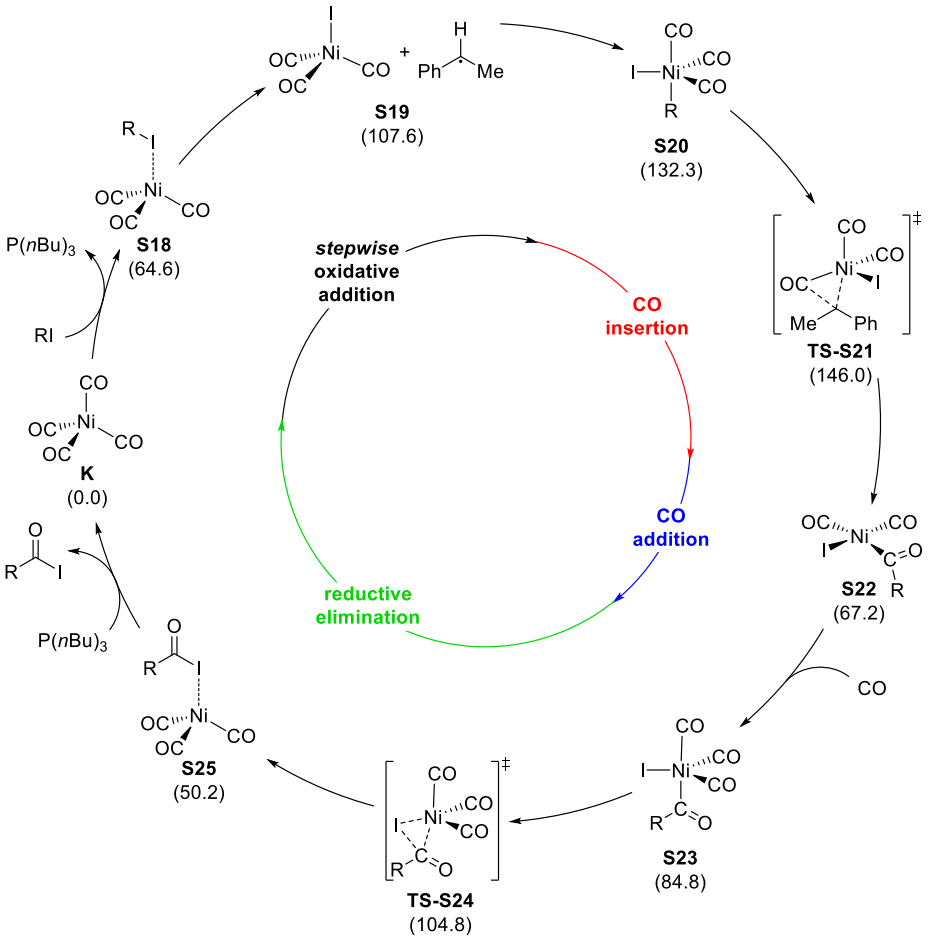

Scheme S6. Catalytic cycle for the carbonylation of RI via 'stepwise' oxidative addition via the Ni(I) complex coordinated by three CO ligands. ΔG^{393} in kJ mol^{-1}; RI-PBE0-D3(BJ)/def2-QZVPP//BP86/def2-SV(P); COSMO-RS (1-phenylethanol).

Similar to the previously investigated mechanistic pathways, the relative energies of 'classical' two-electron oxidative addition transition states were computed (Scheme S7). Oxidative

addition (**TS-S26**; $\Delta G^{\ddagger}$ = 158.7 kJ mol^{-1}) of the alkylhalide to the corresponding adduct complex **S18** forms penta-coordinated complex **S20** (ΔG^{393} = 132.3 kJ mol^{-1}). In agreement with the other mechanistic scenarios, the Ni(I) pathway is favoured over the two-electron oxidative addition.

Overall, the calculations show that the coordination of one equivalent of phosphine will significantly reduce the activation barrier of the carbonylation reaction and the carbonylation is not feasible without the use of phosphine when no LiI is added to the reaction mixture (which is in agreement with the experimental observations).

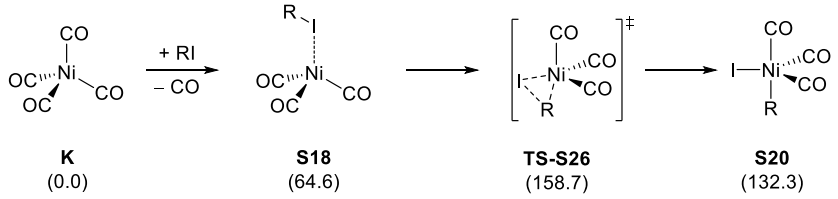

Scheme S7. Reaction pathway for the carbonylation of RI via two-electron oxidative addition via the Ni complex coordinated by three CO ligands. ΔG^{393} in kJ mol^{-1}; RI-PBE0-D3(BJ)/def2-QZVPP//BP86/def2-SV(P); COSMO-RS (1-phenylethanol).

S5.5. Alternative recombination- and radical-reaction pathways

In order to understand the radical reactivity in more detail, a variety of plausible mechanistic pathways after the generation of the Ni(I) species and the phenylethyl radical were probed: (1) The phenylethyl radical can undergo radical recombination with the unpaired electron at the Ni(I) center (**C**). This leads to the formation of pentacoordinated complex **D** (ΔG^{393} = 111.1 kJ mol^{-1}), which can undergo CO insertion (**TS-E**; $\Delta G^{\ddagger}$ = 131.7 kJ mol^{-1}) to form acyl complex **F** (ΔG^{393} = 69.7 kJ mol^{-1}). (2) Addition of the phenylethyl radical to a CO ligand coordinated to the Ni(I) complex (**TS-S27**) could directly lead to the formation of the same acyl complex (**F**; ΔG^{393} = 69.7 kJ mol^{-1}). This transition state could not be located, but geometry optimization lead to surrounding minima even when a promising vibrational mode was present

in the starting structure (from pre-optimization). Based on these observations, we estimate that the transition state energy of this motif is significantly higher than the relative energies of surrounding minima and transition states. (3) Free CO, which should be readily available in the reaction mixture, can add to the phenylethyl radical (**TS-S28**; $\Delta G^{\ddagger}$ = 134.6 kJ mol^{-1}) to form the corresponding acyl radical (ΔG^{393} = 103.4 kJ mol^{-1}). This could consequently recombine with the unpaired electron located on the Ni(I) center and form pentacoordinated species **G** (ΔG^{393} = 75.6 kJ mol^{-1}). However, the formation of the acyl radical (**TS-S28**) is less feasible than the barrierless recombination/CO insertion pathway (see pathway no. 1) and therefore not likely to take place. Furthermore, radical recombination should take place directly after radical formation without any necessity for the radical to escape from the solvent cage, which would be required for CO addition/carbonylation of the radical. This is further supported by the lack of radical recombination side products and low influence of radical inhibitors, which would be expected if an acyl radical outside of the solvent cage would be formed. (4) After hypothetical formation of the acyl radical, the radical could abstract the halide from the Ni(I) complex (in a similar fashion to the initial formation of the same complex) and therefore bypass all 'classical' oxidative addition, CO insertion and reductive elimination transition states altogether. Due to the unfavourable formation of the acyl radical this step was not further investigated in detail. Pathways no. 1 to 3 are all brought to completion via the same reductive elimination step (**TS-H**; $\Delta G^{\ddagger}$ = 106.8 kJ mol^{-1}).

Furthermore, the addition of the phenylethyl radical and acyl radical to the Ni(0) complexes $Ni(CO)_2(TBP)_2$ and $Ni(CO)_3(TBP)$ was investigated to rule out potential side reactions of the radical formation. None of the potential reaction products could be located, but ligand dissociation was observed over the course of the geometry optimization.

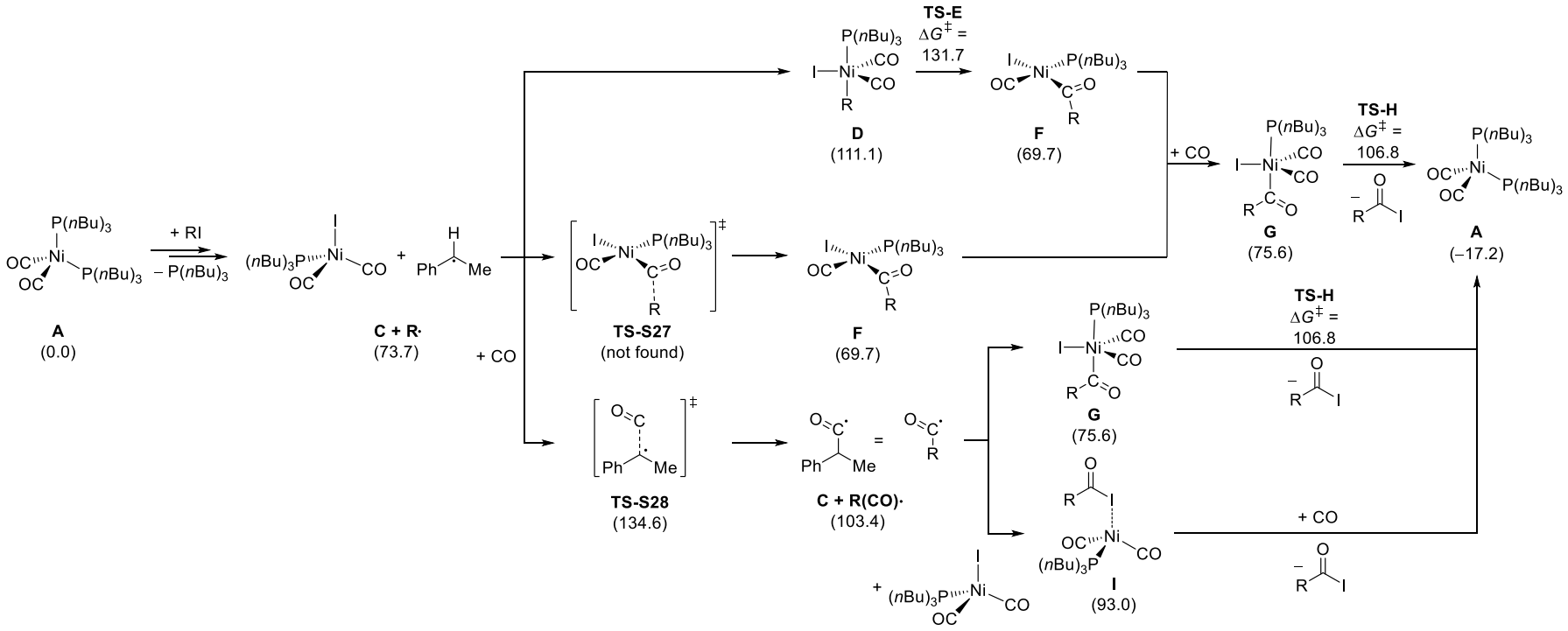

Scheme S8. Possible recombination- and radical-reaction pathways for the catalytic system with a Ni center coordinated by one phosphine and two CO ligands. ΔG^{393} in kJ mol^{-1}; RI-PBE0-D3(BJ)/def2-QZVPP//BP86/def2-SV(P); COSMO-RS (1-phenylethanol).

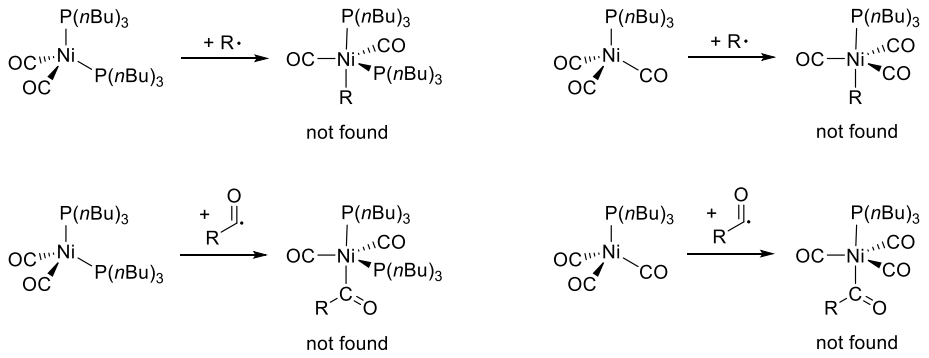

Scheme S9. Possible reaction products for the addition of alkyl or acyl radicals to the Ni(0) complexes $Ni(CO)_2(TBP)_2$ and $Ni(CO)_3(TBP)$. All geometrical isomers of the shown pentacoordinated complexes were attempted to be computed and failed to retain the desired geometry. ΔG^{393} in kJ mol^{-1}; RI-PBE0-D3(BJ)/def2-QZVPP//BP86/def2-SV(P); COSMO-RS (1-phenylethanol).

S5.6. Reaction pathway with the DavePhos ligand coordinated to Ni

When no LiI was employed in the reaction, the use of the DavePhos ligand significantly increased the yield of the desired carbonylation product. Consequently, we adapted the quantum-chemical investigations from the TBP ligand to the DavePhos ligand to see if we could reproduce this effect. As the DavePhos ligand was shown to form a very efficient system in 1:1 ratio to the catalyst (for an explanation, see the section *Ligand screening* in the manuscript), the DavePhos monocoordinated complex **S29** served as starting point for our calculated catalytic cycle (ΔG^{393} = 0.0 kJ mol^{-1}). The mechanistic pathway similarly proceeds via the alkylhalide adduct of the tri-coordinated $Ni(CO)_2L$ complex (**S30**; ΔG^{393} = 69.8 kJ mol^{-1}) and the formation of the Ni(I) species **S31** (and phenylethyl radical) (ΔG^{393} = 63.0 kJ mol^{-1}). Barrierless addition to the of the radical to Ni(I) complex **S31** yields pentacoordinated complex **S32** (ΔG^{393} = 106.4 kJ mol^{-1}), which can undergo CO-insertion (**TS-S33**; $\Delta G^{‡}$ = 129.3 kJ mol^{-1}) to form **S34** (ΔG^{393} = 60.4 kJ mol^{-1}). Addition of a CO molecule will yield pentacoordinated complex **S35** (ΔG^{393} = 82.6 kJ mol^{-1}). Finally, reductive elimination (**TS-**

S36; $\Delta G^{\ddagger} = 90.9$ kJ mol^{-1}) will afford the adduct complex **S37** bearing the carbonylated product ($\Delta G^{393} = 63.7$ kJ mol^{-1}), which dissociates to close the catalytic cycle.

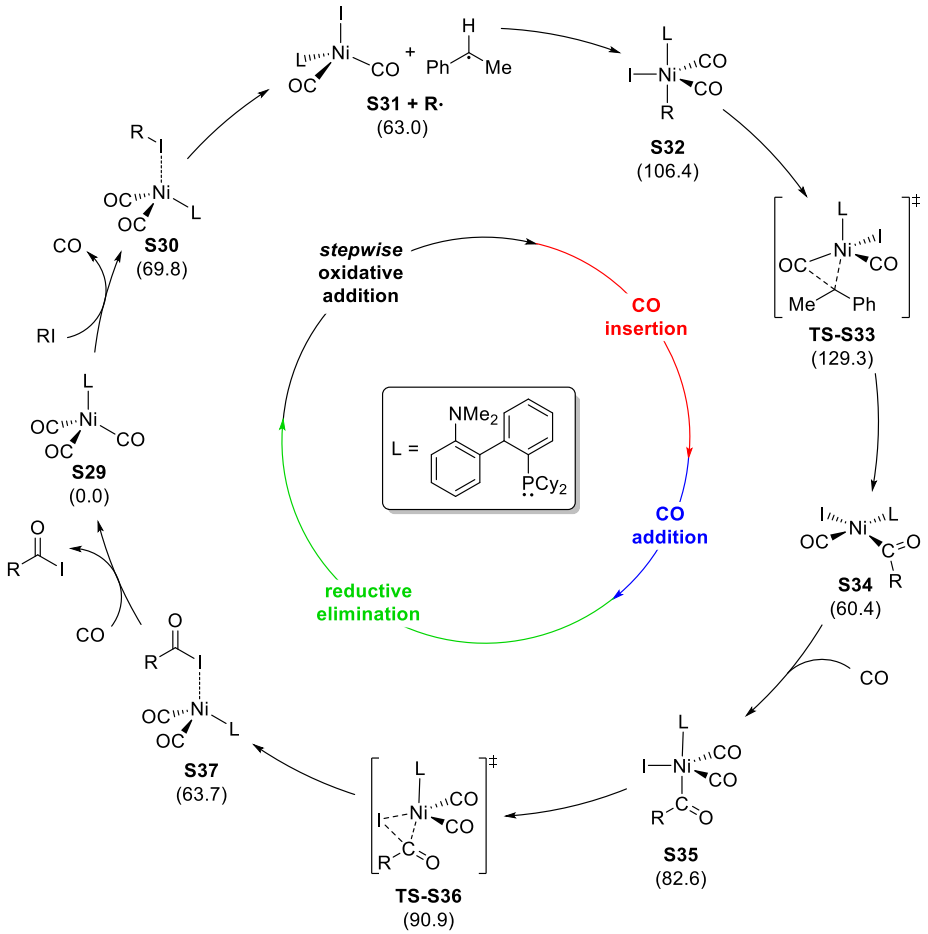

Scheme S10. Catalytic cycle for the carbonylation of RI via 'stepwise' oxidative addition via the Ni(I) complex coordinated by DavePhos and two CO ligands. ΔG^{393} in kJ mol^{-1}; RI-PBE0-D3(BJ)/def2-QZVPP//BP86/def2-SV(P); COSMO-RS (1-phenylethanol).

The 'classical' two-electron oxidative addition with CO insertion pathway was also investigated for the DavePhos ligand (Scheme S11). Although the activation barrier for oxidative addition (**TS-S38**; $\Delta G^{\ddagger} = 184.8$ kJ mol^{-1}) is lower than the corresponding transition state for the TBP ligand (see Scheme 8) or the other investigated systems, the activation energy is still too high to be feasible at the employed reaction conditions. Once more, the Ni(I) pathway proved to be significantly favoured over the 'classical' pathway (cf. Scheme S10).

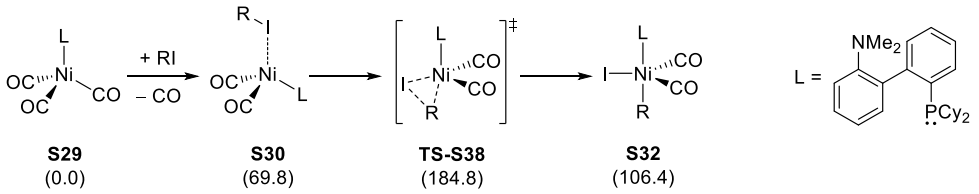

Scheme S11. Reaction pathway for the carbonylation of RI via two-electron oxidative addition via the Ni complex coordinated by DavePhos and two CO ligands. ΔG^{393} in kJ mol^{-1}; RI-PBE0-D3(BJ)/def2-QZVPP//BP86/def2-SV(P); COSMO-RS (1-phenylethanol).

S5.7. Reaction pathway with the depe ligand coordinated to Ni

The experimental observations (when not employing LiI) show that the chelating bidentate ligands like dppe or similar show a significantly reduced activity. Therefore, the previously determined pathways were also studied for the depe ligand (ethyl groups were used to reduce the size of the computed model system). Similar to the previously investigated system bearing two monodentate TBP ligands (cf. Section S5.3), the mechanistic pathway begins with formation of the alkylhalide adduct of the tricoordinate Ni(CO)(depe) species (**S40**; ΔG^{393} = 128.6 kJ mol^{-1}), which will subsequently lead to phenylethyl radical and Ni(I) complex formation (**S41**; ΔG^{393} = 48.1 kJ mol^{-1}). Barrierless addition of the radical to the Ni(I) complex **S41** will form the pentacoordinated complex **S42** (ΔG^{393} = 64.7 kJ mol^{-1}). CO-insertion (**TS-S43**; $\Delta G^{\ddagger}$ = 79.0 kJ mol^{-1}) takes place to yield tetracoordinated acyl nickel complex **S44** (ΔG^{393} = 14.9 kJ mol^{-1}), which adds further CO resulting in pentacoordinated species **S45** (ΔG^{393} = 23.5 kJ mol^{-1}). The catalytic cycle will be completed by reductive elimination of R(CO)I from the Ni complex (**TS-S46**; $\Delta G^{\ddagger}$ = 94.9 kJ mol^{-1}). Surprisingly, the energy barrier for the rate-determining step is only slightly higher than for the previously calculated carbonylation with the Ni(CO)$_3$(TBP) system.

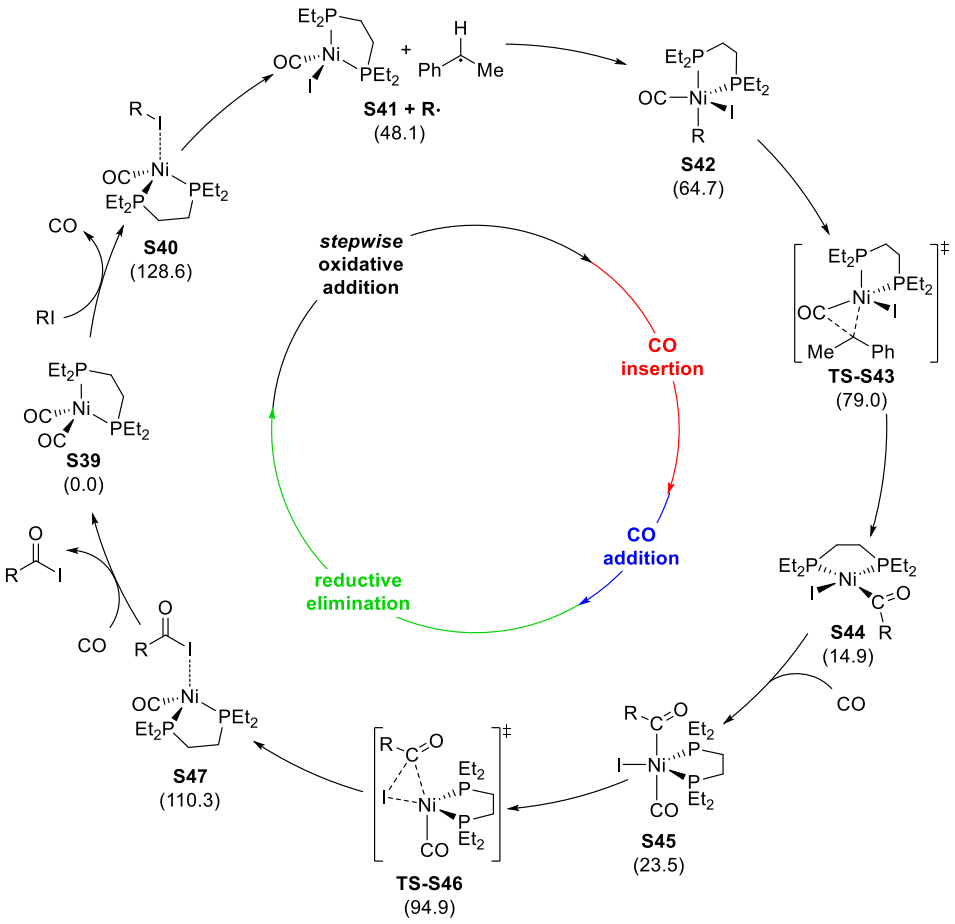

Scheme S12. Catalytic cycle for the carbonylation of RI via 'stepwise' oxidative addition via the Ni(I) complex coordinated by depe and one CO ligand. ΔG^{393} in kJ mol^{-1}; RI-PBE0-D3(BJ)/def2-QZVPP//BP86/def2-SV(P); COSMO-RS (1-phenylethanol).

As the reference structure **S39** (ΔG^{393} = 0.0 kJ mol^{-1}) might incorporate the depe ligand with a significant strain/distortion (a(P–Ni–P) = 90° in a tetragonal coordination geometry), which could strongly distort the results for the investigated mechanistic pathway, a closer look was taken at the reduction step, that was assumed to yield said complex (**S39**; see Scheme S13). This formation could proceed via a $NiI_2(TBP)_2$ species for the TBP ligand and via the equivalent $Ni(depe)I_2$ species when employing depe. While the monodentate nature of the TBP ligand enables the formation of *cis*- (**S49**) and *trans*-complexes (**S48**), the chelating depe ligand is restricted to a *cis*-geometry (**S50**). The *trans* TBP-complex is more stable than its *cis* counterpart and reduction to $Ni(CO)_2(TBP)_2$ (**A**) is strongly exergonic (ΔG^{393} =

−23.9 kJ mol^{-1}). On the other hand, the reduction of Ni(depe)I_2 (**S50**) to Ni(CO)2(depe) (**S39**) was computed to be endergonic (ΔG^{393} = 27.5 kJ mol^{-1}). When comparing the two cis complexes for TBP (**S49**) and depe (**S50**), this is even more pronounced and the reduction step is significantly less favoured for the depe system, which is most likely a representation of the unfavourable strain in complex **S39**.

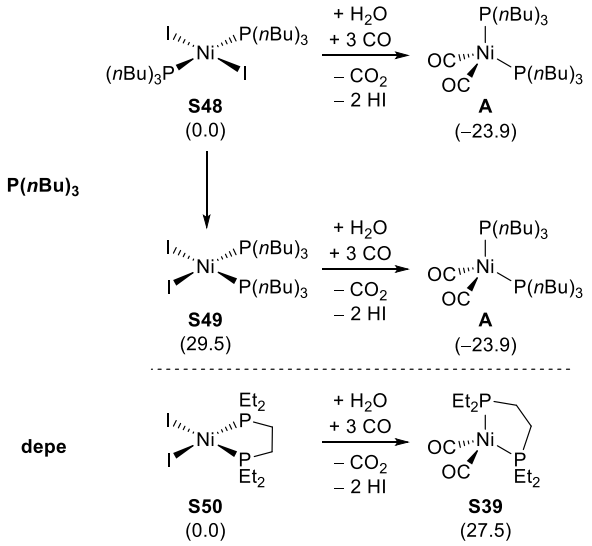

Scheme S13. Computed thermodynamic stabilities for the formation of $Ni(CO)_2(TBP)_2$ and $Ni(CO)_2$(depe) via a Ni(II) to Ni(0) reduction step . ΔG^{393} in kJ mol^{-1}; RI-PBE0-D3(BJ)/def2-QZVPP//BP86/def2-SV(P); COSMO-RS (1-phenylethanol).

This is in agreement with the result, that even when employing LiI, which should enable a ligand-free pathway the activity does not match the activity of TBP (or similar monodentate ligands) as the original formation of a Ni(0) might be hindered when employing depe and therefore further increase the activation energy.

To further study these effects and explain the varying reactivity when extending the backbone length of the chelating ligand, the initial reduction step was recalculated for a variety of ligands bearing different substituents and incorporating different backbone lengths (n=2-3; see Table S1).

Again, these are in qualitative agreement with experiments: (1) The use of dppe results in better yields compared to dcpe, which was found to be more endergonic in the reduction step. (2) Increasing the length of the backbone of the chelating ligand will significantly reduce the relative energy of the Ni(0) product of the reduction step.

Table S8. Computed free Gibbs energies of reaction for the reduction of $NiLI_2$ to $Ni(CO)_2L$ for a selection of bidentate ligands.

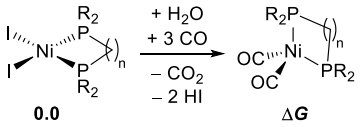

L	R	n	Δ*G*
depe	Et	2	27.5
dcpe	Cy	2	50.0
dppe	Ph	2	3.0
depp	Et	3	11.0
dippp	^{i}Pr	3	–11.0
dcpp	Cy	3	6.8
dppp	Ph	3	–10.9

S5.8. Two-electron oxidative addition pathway in the anionic regime

In order to further ensure that the anionic Ni(I)-based mechanistic pathway (see Scheme 8) presents the most favourable pathway, the 'classical' two-electron oxidative addition transition state in the anionic regime was investigated (Scheme S14). Despite all efforts, the oxidative addition transition state could not be located indicating that it is considerably higher in relative energy than the surrounding structures which were obtained after geometry optimization. Due to the high activation barrier for the two-electron oxidative addition, the mechanistic pathway via Ni(I) (see Scheme 8) is proposed.

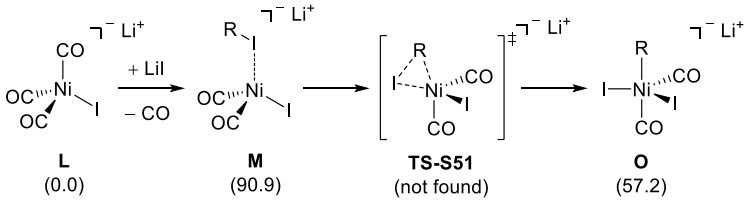

Scheme S14. Reaction pathway for the carbonylation of RI via two-electron oxidative addition via the anionic Ni complex coordinated by three CO ligands. ΔG^{393} in kJ mol^{-1}; RI-PBE0-D3(BJ)/def2-QZVPP//BP86/def2-SV(P); COSMO-RS (1-phenylethanol).

S5.9. Alternative recombination- and radical-reaction pathways in the anionic regime

Similar to the investigations of the neutral phosphine-stabilized pathways, an in-depth evaluation of potential reaction pathways after the phenylethyl radical generation was carried out (Scheme S15). After generation of the free radical (ΔG^{393} = 29.9 kJ mol^{-1}) the same four pathways could occur: (1) Barrierless recombination of Ni(I) and the radical followed by CO insertion (**TS-S52**; $\Delta G^{\ddagger}$ = 77.0 kJ mol^{-1}). (2) Addition of the phenylethyl radical to one of the CO ligands of the Ni(I) complex (**TS-S28**). (3) Barrierless recombination of the Ni(I) complex and an acyl radical. (4) Abstraction of iodine from the Ni(I) complex by an acyl radcial. Pathway (3) and (4) would require initial formation of the acyl radical which was determined to be unfavourable. Therefore, we propose that radical recombination will directly place after the radical's formation, which is also in accordance with our (lack of) experimental observations regarding other potential recombination products that should be observed when acyl radical formation takes place.

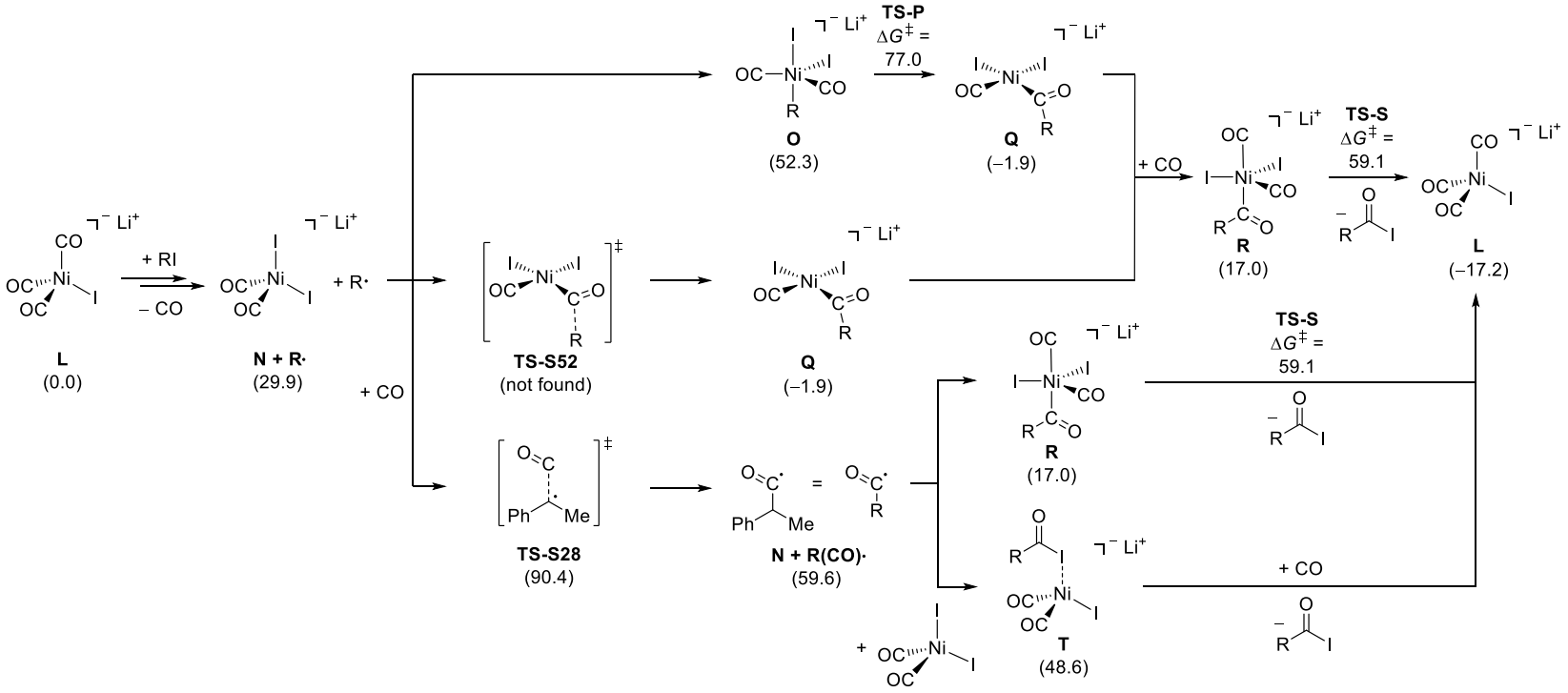

Scheme S15. Possible recombination- and radical-reaction pathways for the catalytic system with an anionic Ni center coordinated by three CO ligands. ΔG^{393} in kJ mol^{-1}; RI-PBE0-D3(BJ)/def2-QZVPP//BP86/def2-SV(P); COSMO-RS (1-phenylethanol).

S5.10. Coordination of phosphine to Ni in the anionic regime

In order to investigate whether the addition of phosphine could influence the proposed anionic reaction pathway, the substitution of one of the CO ligands by TBP was investigated. Interestingly, the substitution of CO by the phosphine does not lead to a significant increase in relative energy and consequently opens up the possibility for a mechanistic scenario similar to the one previously studied without the involvement of phosphine. Formation of the RI adduct **S54** (ΔG^{393} = 106.3 kJ mol^{-1}), the Ni(I) species **S55** and radical (ΔG^{393} = −4.9 kJ mol^{-1}) and a tetradentate Ni(II) acyl complex (**S58**; ΔG^{393} = −9.6 kJ mol^{-1}) are followed by CO addition to form the pentacoordinated complex **S59** (ΔG^{393} = −7.6 kJ mol^{-1}). Reductive elimination transition state **TS-S60** ($\Delta G^{‡}$ = 91.1 kJ mol^{-1}) enables formation of the R(CO)I adduct **S61** (ΔG^{393} = 87.0 kJ mol^{-1}) and consequently product formation.

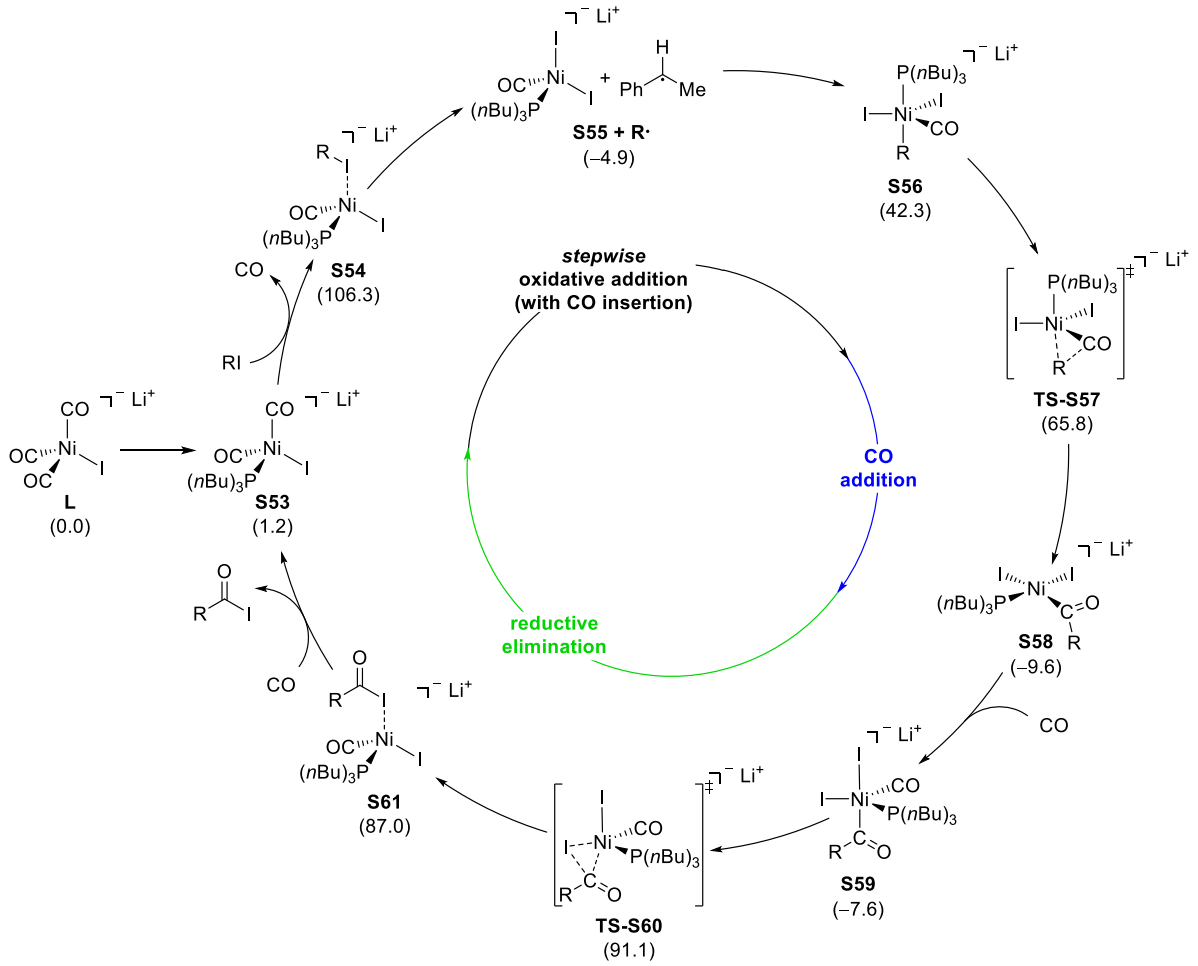

Scheme S16. Catalytic cycle for the carbonylation of RI via 'stepwise' oxidative addition via the Ni(I) complex coordinated by depe and one CO ligand. ΔG^{393} in kJ mol^{-1}; RI-PBE0-D3(BJ)/def2-QZVPP//BP86/def2-SV(P); COSMO-RS (1-phenylethanol).

S5.11. Coordination of methyl ethyl ketone to the Ni center

In order to exclude the possibility of methyl ethyl ketone being involved as a ligand, a variety of ketone-coordinated complexes was investigated. The combination of 14 structural motives for potential ketone complexes, two coordination modes (η^1 or η^2) and multiple conformers resulted in 68 different investigated complexes. Many of these complexes resulted in immediate ketone dissociation over the course of the geometry optimization. The change of energy during the optimization clearly shows that the non ketone-coordinated complex is significantly more stable. Seven different neutral (phosphine-coordinated pathway) and four different anionic (LiI-induced pathway) complexes were identified, which could serve as precursor to ketone addition: **A**, **S7**, **K**, **S4**, **S5**, **S66**, and **C** (neutral; see Scheme S17) as well as **K**, **L**, **S73**, and **N** (anionic; see Scheme S18). While not all of the geometry optimizations lead to the dissociation of the ketone ligand, the ketone addition led to higher Gibbs free energies for all investigated cases (relative to the non-ketone precursor). The Gibbs free energy difference is at least 26.0 kJ mol^{-1} for the addition of MEK to **S66** (yielding **S67**) and reaches up to 87.8 kJ mol^{-1} for the formation of **S70** from **C**.

Therefore, it was concluded that the ketone solvent is not involved as ligand in the reaction mechanism but is only providing better solubility.

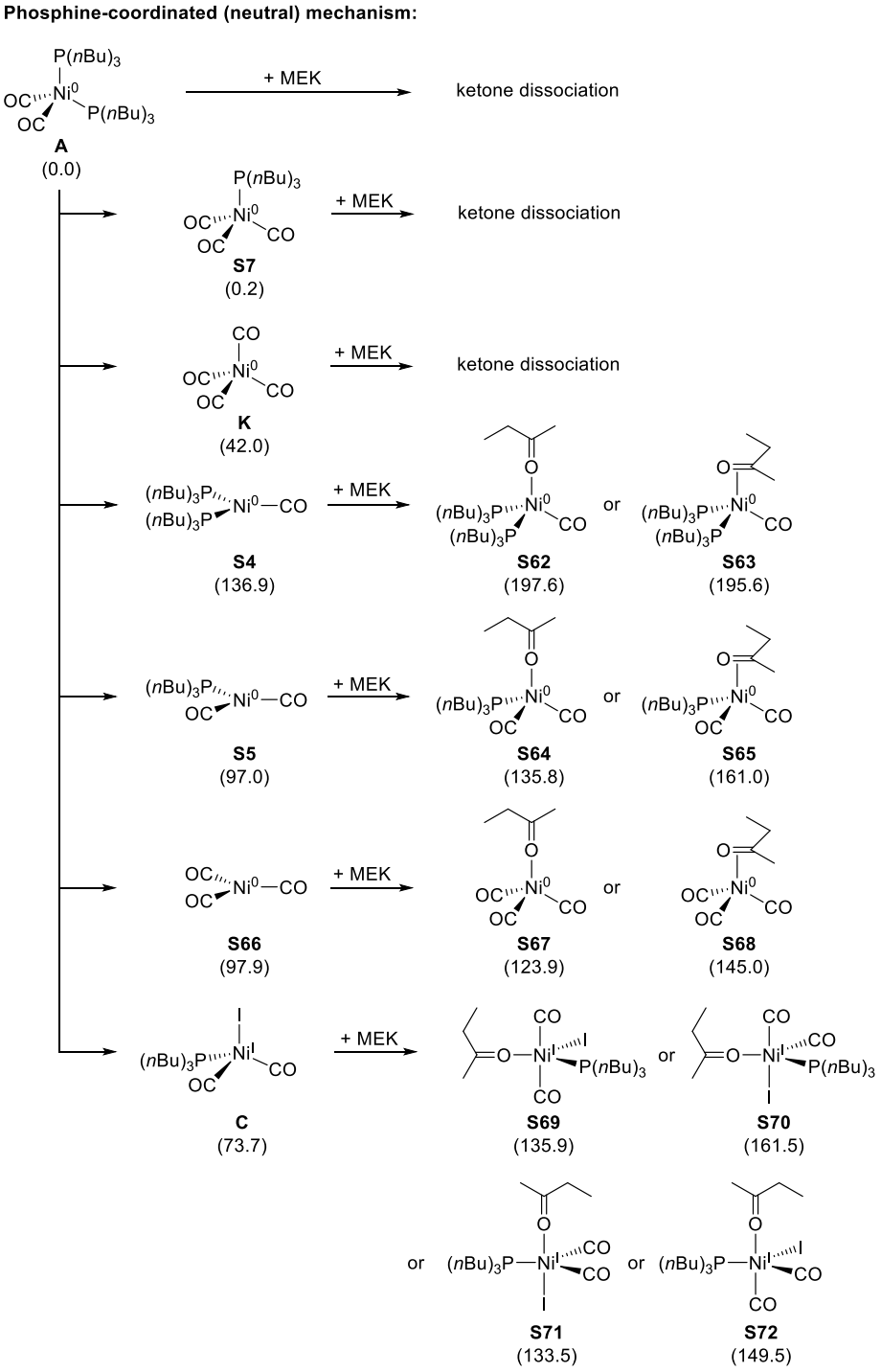

Scheme S17. Relative energies for the coordination of methyl ethyl ketone to neutral Ni complexes. ΔG^{393} in kJ mol^{-1}; RI-PBE0-D3(BJ)/def2-QZVPP//BP86/def2-SV(P); COSMO-RS (1-phenylethanol).

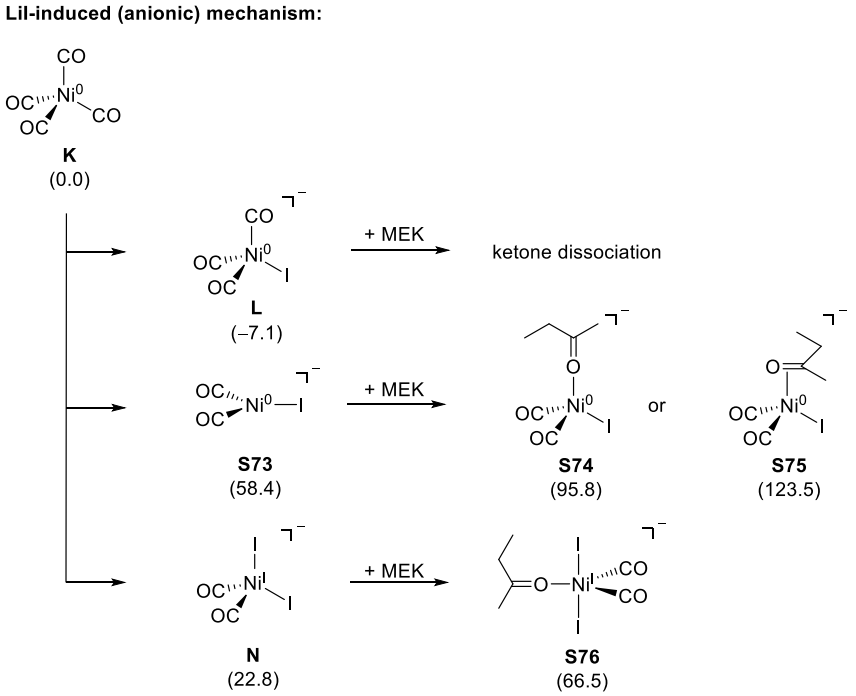

Scheme S18. Relative energies for the coordination of methyl ethyl ketone to anionic Ni complexes. ΔG^{393} in kJ mol^{-1}; RI-PBE0-D3(BJ)/def2-QZVPP//BP86/def2-SV(P); COSMO-RS (1-phenylethanol).

S5.12. Generation of stabilized two-coordinate Ni(0) complexes

The possibility of generating a stabilized two-coordinate Ni(0) complex (**S77**, **S78**, or **S79**), that could further undergo oxidative addition of the alkyl halide to form tetra-coordinate Ni(II) complexes, was also investigated. However, the stabilized two-coordinate complexes (similar to the respective unstabilized complexes) are exhibiting a too high relative energy to be relevant for the reaction mechanism. The stability of these adducts decreases with higher amounts of TBP ligands coordinated to the Ni center leading to **S79** being the most stable of the three structures (ΔG^{393} = 164.3 kJ mol^{-1}).

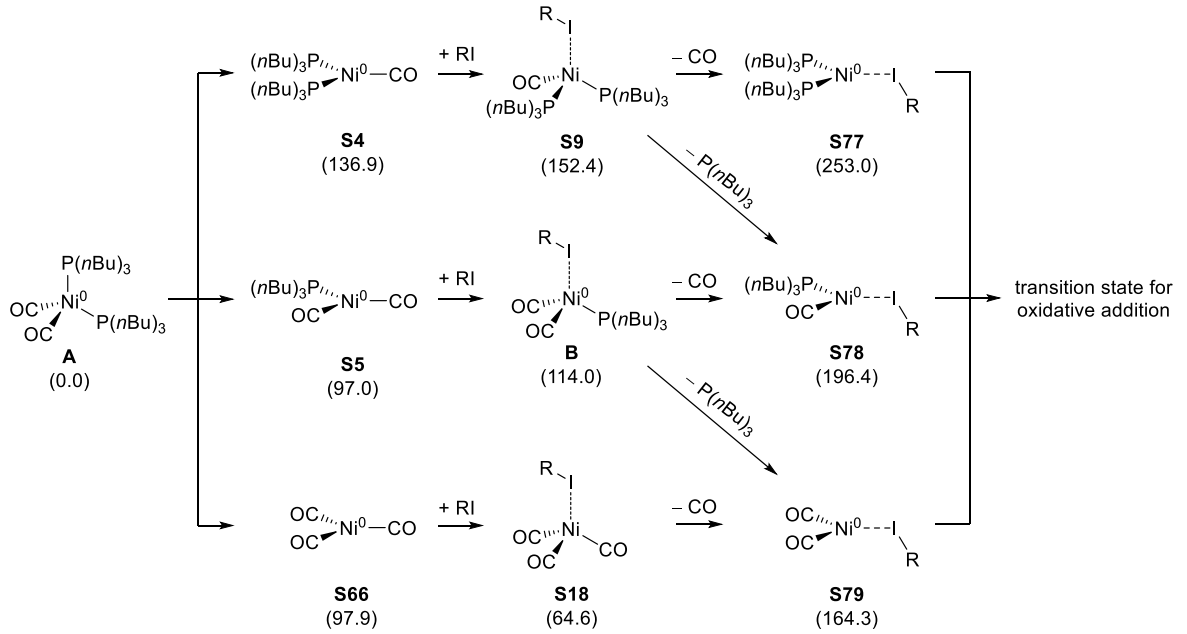

Scheme S19. Relative energies for the generation of stabilized two-coordinate Ni(0) complexes via ligand dissociation of the respective three-coordinate complex. ΔG^{393} in kJ mol^{-1}; RI-PBE0-D3(BJ)/def2-QZVPP//BP86/def2-SV(P); COSMO-RS (1-phenylethanol).

S5.13. Reactivity of the generated alkyl radical towards Ni(0) complexes

In order to investigate the possibility of the generated alkyl radicals adding to tri-coordinate complexes (i.e. **S4**, **S5**, **S66**, or **S73**) various pathways to generate these two species were investigated. All the possibilities to generate both a tri-coordinate complex and the alkyl radical (with the corresponding Ni(I) species formed in the process) show high relative energies (ΔG^{393} = 95.4 – 247.1 kJ mol^{-1}). On the contrary, in the proposed mechanistic pathways (vide supra) only one of these two unfavourable species has to be formed at a time leading to a significantly lower activation barrier for these pathways. Furthermore, addition of **R•** is only exergonic for the addition to **S4** (**S80**; ΔG^{R} = −4.1 kJ mol^{-1}). The addition of **R•** gets more endergonic the more CO ligands are coordinated to the tri-coordinate structure (**S81**: ΔG^{R} = 16.8 kJ mol^{-1}; **S82**: ΔG^{R} = 26.4 kJ mol^{-1}). All in all, neither the here presented addition nor addition to the tetra-coordinate complexes (**A**, **S7**, or **K**; vide supra) does present a viable alternative to the mechanism presented in this work.

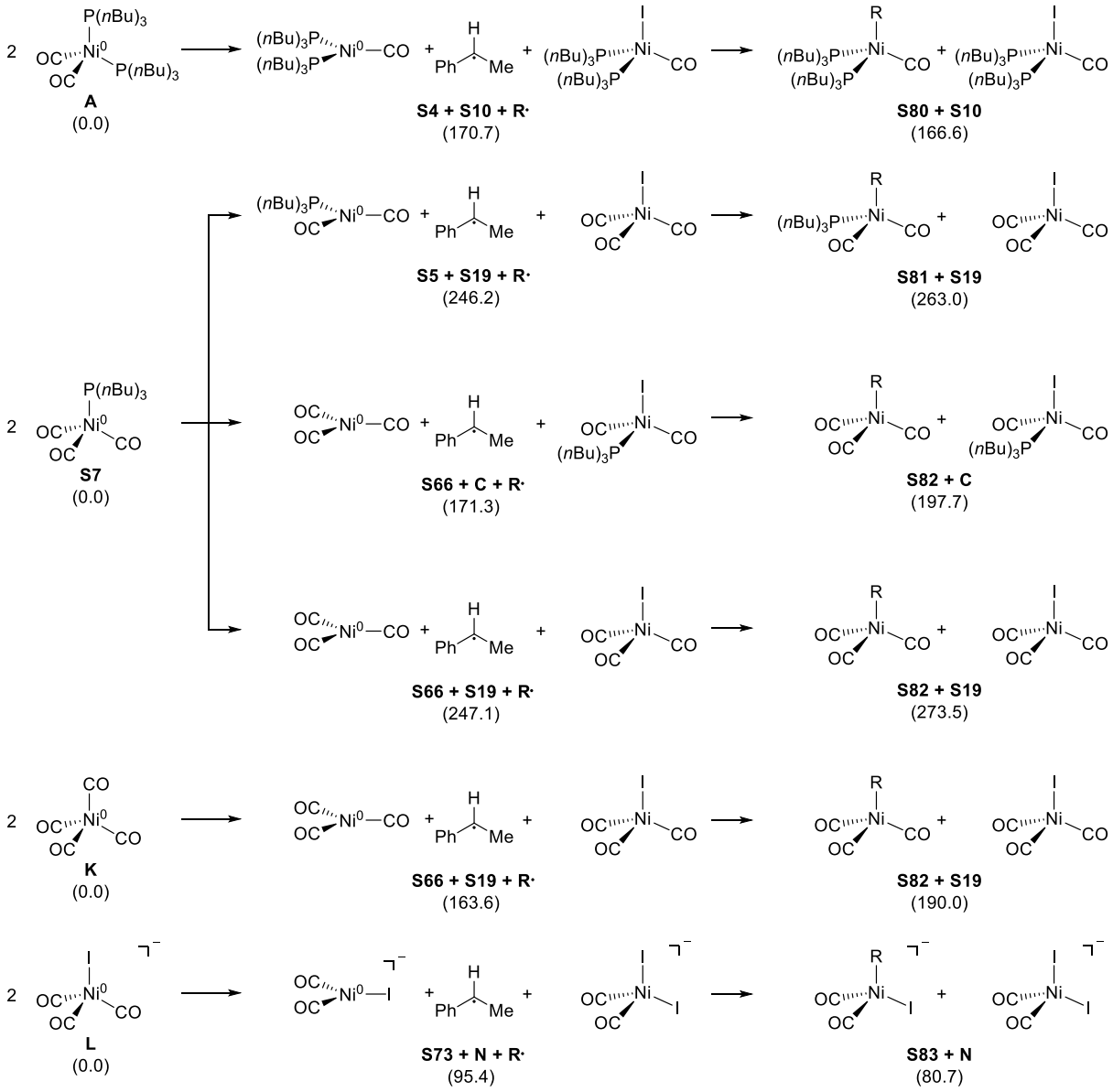

Scheme S20. Relative energies for the addition of alkyl radicals to the three-coordinate Ni(0) complexes. ΔG^{393} in kJ mol^{-1}; RI-PBE0-D3(BJ)/def2-QZVPP//BP86/def2-SV(P); COSMO-RS (1-phenylethanol).

S6. Characterization data

S6.1. Characterization data of benzylic alcohols

2-phenylpropanoic acid

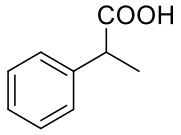

Synthesized following the general procedure for the carbonylation of benzylic alcohols (Procedure A). Colorless oil, isolated yield: 82%, 1.02 g. Rf = 0.4 (0 to 30% EtOAc in petroleum ether). ^{1}H NMR (301 MHz, $CDCl_3$): δ 11.60 (br s, 1H), 7.46 – 7.25 (m, 5H), 3.79 (q, J = 7.2 Hz, 1H), 1.56 (d, J = 7.2 Hz, 3H). $^{13}C\{^{1}H\}$ NMR (76 MHz, $CDCl_3$): δ 181.2, 139.8, 128.7, 127.7, 127.5, 45.5, 18.1. Anal. Calcd. for $C_9H_{10}O_2$ (150.18 g/mol): C, 71.98; H, 6.71. Found: C, 72.16; H, 6.91.

2-(4-isobutylphenyl)propanoic acid

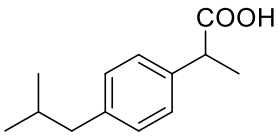

Synthesized following the general procedure for the carbonylation of benzylic alcohols (Procedure A). White solid, isolated yield: 52%, 890.3 mg. Rf = 0.45 (0 to 25% EtOAc in petroleum ether). ^{1}H NMR (301 MHz, $CDCl_3$): δ 11.17 (br s, 1H), 7.43 (d, J = 8.1 Hz, 2H), 7.31 (d, J = 8.1 Hz, 2H), 3.92 (q, J = 7.1 Hz, 1H), 2.66 (d, J = 7.2 Hz, 2H), 2.06 (dp, J = 13.5, 6.7 Hz, 1H), 1.71 (d, J = 7.2 Hz, 3H), 1.11 (d, J = 6.6 Hz, 6H). $^{13}C\{^{1}H\}$ NMR (76 MHz, $CDCl_3$): δ 181.1, 140.9, 137.0, 129.4, 127.3, 45.1, 45.0, 30.2, 22.4, 18.1. Anal. Calcd. for $C_{13}H_{18}O_2$ (206.28 g/mol): C, 75.69; H, 8.80. Found: C, 75.99; H, 8.83.

2-(6-methoxynaphthalen-2-yl)propanoic acid

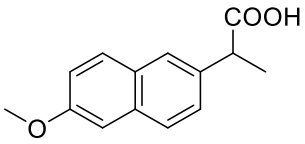

Synthesized following the general procedure for the carbonylation of benzylic alcohols (Procedure A). Light yellow solid, isolated yield: 26%, 90 mg (the reaction was performed with 1.5 mmol starting material and 2 mL MEK). Rf = 0.33 (0 to 40% EtOAc in petroleum ether). ^{1}H NMR (301 MHz, $CDCl_3$): δ 7.70 (m, 3H), 7.42 (dd, J = 8.4, 1.9 Hz, 1H), 7.13 (m, 2H), 3.91 (s, 3H), 3.86 (q, J = 7.3 Hz, 1H), 1.60 (d, J = 7.2 Hz, 3H) [acid proton not visible due to fast exchange]. ^{13}C{^{1}H} NMR (76 MHz, $CDCl_3$): δ 180.6, 157.73, 134.9, 133.8, 129.3, 128.9, 127.2, 126.2, 126.1, 119.0, 105.6, 55.3, 45.3, 18.1. Anal. Calcd. for $C_{14}H_{14}O_3$ (230.26 g/mol): C, 73.03; H, 6.13. Found: C, 73.19; H, 6.11.

2-(p-tolyl)propanoic acid

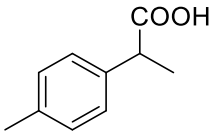

Synthesized following the general procedure for the carbonylation of benzylic alcohols (Procedure A). Colorless oil, isolated yield: 59%, 804.1 mg. Rf = 0.4 (0 to 30% EtOAc in petroleum ether). ^{1}H NMR (301 MHz, $CDCl_3$): δ 10.79 (br s, 1H), 7.26 – 7.11 (m, 4H), 3.72 (q, J = 7.2 Hz, 1H), 2.35 (s, 3H), 1.51 (d, J = 7.2 Hz, 3H). ^{13}C{^{1}H} NMR (76 MHz, CDCl3): δ 181.1, 137.1, 136.8, 129.4, 127.5, 44.9, 21.1, 18.1. Anal. Calcd. for $C_{10}H_{12}O_2$ (164.20 g/mol): C, 73.15; H, 7.37. Found: C, 73.34; H, 7.34.

2-(4-(trifluoromethyl)phenyl)propanoic acid

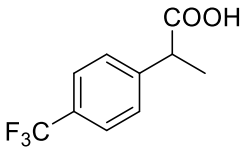

Synthesized following the general procedure for the carbonylation of benzylic alcohols (Procedure A). Light yellow solid, isolated yield: 57%, 1.03 g. Rf = 0.4 (0 to 30% EtOAc in petroleum ether). ^{1}H NMR (301 MHz, $CDCl_3$): δ 10.97 (br s, 1H), 7.60 (d, J = 8.2 Hz, 2H), 7.45 (d, J = 8.3 Hz, 2H), 3.82 (q, J = 7.2 Hz, 1H), 1.55 (d, J = 7.2 Hz, 3H). ^{13}C{^{1}H} NMR (76 MHz, $CDCl_3$): δ 180.4, 143.6, 129.8 (q, J = 32.5 Hz), 128.1, 125.6 (q, J = 3.8 Hz), 124.1 (d, J = 272.0 Hz), 45.3, 17.9. ^{19}F NMR (283 MHz, $CDCl_3$): δ -62.6 (s). Anal. Calcd. for $C_{10}H_9F_3O_2$ (218.17 g/mol): C, 55.05; H, 4.16. Found: C, 55.30; H, 4.37.

2-phenylbutanoic acid

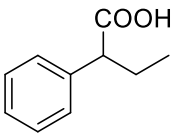

Synthesized following the general procedure for the carbonylation of benzylic alcohols (Procedure A). Colorless oil, isolated yield: 43%, 586 mg. Rf = 0.4 (0 to 30% EtOAc in petroleum ether). ^{1}H NMR (301 MHz, $CDCl_3$): δ 11.25 (br s, 1H), 7.39 – 7.28 (m, 5H), 3.50 (t, J = 7.7 Hz, 1H), 2.30 – 2.02 (m, 1H), 1.98 – 1.73 (m, 1H), 0.95 (t, J = 7.4 Hz, 3H). ^{13}C{^{1}H} NMR (76 MHz, $CDCl_3$): δ 180.6, 138.4, 128.7, 128.1, 127.5, 53.4, 26.3, 12.1. Anal. Calcd. for $C_{10}H_{12}O_2$ (164.20 g/mol): C, 73.15; H, 7.37. Found: C, 72.86; H, 7.49.

2,3-dihydro-1H-indene-1-carboxylic acid

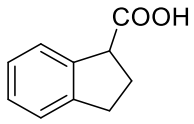

Synthesized following the general procedure for the carbonylation of benzylic alcohols (Procedure A). White solid, isolated yield: 19%, 256 mg. Rf = 0.4 (0 to 30% EtOAc in petroleum ether). ^{1}H NMR (301 MHz, $CDCl_3$): δ 11.63 (brs, 1H), 7.50 – 7.42 (m, 1H), 7.31 – 7.19 (m, 3H), 4.13 (dd, J = 8.2, 6.3 Hz, 1H), 3.21 – 3.10 (m, 1H), 3.04 – 2.90 (m, 1H), 2.57 – 2.31 (m, 2H). ^{13}C{^{1}H} NMR (76 MHz, $CDCl_3$) δ 180.7, 144.2, 140.1, 127.8, 126.6, 125.0, 124.7, 50.1, 31.7, 28.7. Anal. Calcd. for $C_{10}H_{10}O_2$ (162.19 g/mol): C, 74.06; H, 6.22. Found: C, 73.87; H, 6.27.

2-phenylacetic acid

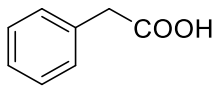

Synthesized following the general procedure for the carbonylation of benzylic alcohols (Procedure A). White crystalline solid, isolated yield: 90%, 1.02 g. Rf = 0.4 (0 to 30% EtOAc in petroleum ether). ^{1}H NMR (301 MHz, $CDCl_3$): δ 11.75 (br s, 1H), 7.46 – 7.29 (m, 5H), 3.71 (s, 2H). ^{13}C{^{1}H} NMR (76 MHz, $CDCl_3$): δ 178.4, 133.3, 129.5, 128.7, 127.4, 41.1. Anal. Calcd. for $C_8H_8O_2$ (136.15 g/mol): C, 70.58; H, 5.92. Found: C, 70.65; H, 5.98.

S6.2. Characterization data of aliphatic alcohols

Cyclohexanecarboxylic acid

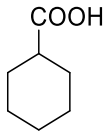

Synthesized following the general procedure for the carbonylation of aliphatic alcohols (Procedure B); 2 equiv. of H_2O was used for the reaction. Colorless oil, isolated yield: 83%, 883 mg. Rf = 0.4 (0 to 20% EtOAc in petroleum ether). ^{1}H NMR (301 MHz, $CDCl_3$): δ 11.38 (brs, 1H), 2.33 (tt, J = 11.1, 3.6 Hz, 1H), 1.93 (dd, J = 12.9, 2.5 Hz, 2H), 1.83 – 1.69 (m, 2H), 1.69 – 1.57 (m, 1H), 1.55 – 1.37 (m, 2H), 1.37 – 1.17 (m, 3H). ^{13}C{^{1}H} NMR (76 MHz, $CDCl_3$): δ 182.8, 42.9, 28.7, 25.7, 25.3. Anal. Calcd. for $C_7H_{12}O_2$ (128.17 g/mol): C, 65.60; H, 9.44. Found: C, 65.50; H, 9.34.

Cyclooctanecarboxylic acid

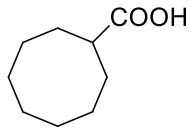

Synthesized following the general procedure for the carbonylation of aliphatic alcohols (Procedure B); 2 equiv. of H_2O was used for the reaction. Colorless oil, isolated yield: 92%, 1.193 g. Rf = 0.4 (0 to 20% EtOAc in petroleum ether). ^{1}H NMR (301 MHz, $CDCl_3$): δ 10.90 (brs, 1H), 2.63 – 2.46 (m, 1H), 2.03 – 1.84 (m, 2H), 1.84 – 1.63 (m, 4H), 1.63 – 1.43 (m, 8H). ^{13}C{^{1}H} NMR (76 MHz, $CDCl_3$): δ 183.9, 43.4, 28.4, 26.8, 26.1, 25.1. Anal. Calcd. for $C_9H_{16}O_2$ (156.22 g/mol): C, 69.19; H, 10.32. Found: C, 68.92; H, 10.42.

3-phenylpropanoic acid

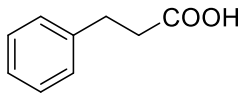

Synthesized following the general procedure for the carbonylation of aliphatic alcohols (Procedure B); 1 equiv. of H_2O was used for the reaction. Pale yellow viscous oil, combined isolated yield: 56%, 698 mg (1:2, b:l); distinct signals of linear isomer are marked * and those of branched **. Rf = 0.4 (0 to 30% EtOAc in petroleum ether). ^{1}H NMR (301 MHz, $CDCl_3$): δ 10.97 (brs, 3H, overlapping), 7.62 – 6.92 (m, 15H, overlapping), 3.79** (q, J = 7.2 Hz, 1H), 3.00* (t, J = 7.8 Hz, 4H), 2.79 – 2.67* (m, 4H), 1.57** (d, J = 7.2 Hz, 3H). ^{13}C{^{1}H} NMR (76 MHz, $CDCl_3$): δ 180.9**, 179.4*, 140.2*, 139.8**, 128.7**, 128.6*, 128.3*, 127.6**, 127.4**, 126.4*, 45.4**, 35.6*, 30.6*, 18.1**. Anal. Calcd. for $C_9H_{10}O_2$ (150.18 g/mol): C, 71.98; H, 6.71. Found: C, 71.71; H, 6.70.

Propionic acid

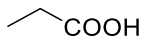

Synthesized following the general procedure for the carbonylation of aliphatic alcohols (Procedure B); No H_2O was used for the reaction. Colorless liquid, isolated yield: 64%, 394 mg. Rf = 0.4 (0 to 25% EtOAc in petroleum ether). ^{1}H NMR (301 MHz, $CDCl_3$): δ 10.85 (br s, 1H), 2.49 – 2.14 (m, 2H), 1.09 (t, J = 7.6 Hz, 3H). ^{13}C{^{1}H} NMR (76 MHz, $CDCl_3$): δ 180.9, 27.4, 8.8.

Isobutyric acid

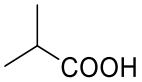

Synthesized following the general procedure for the carbonylations of aliphatic alcohols (Procedure B); No H_2O was used for the reaction. Colorless liquid, combined isolated yield: 74%, 541 mg (1:1, b:l); distinct signals of branched isomer are marked * and those of linear **. Rf = 0.4 (0 to 25% EtOAc in petroleum ether). ^{1}H NMR (301 MHz, $CDCl_3$) δ 11.21 (br s, 2H, overlapping), 2.71 – 2.51* (m, 1H), 2.35** (t, J = 7.4 Hz, 2H), 1.80 – 1.59** (m, 2H), 1.21* (d, J = 7.0 Hz, 6H), 0.99** (t, J = 7.4 Hz, 3H). $^{13}C\{^1H\}$ NMR (76 MHz, $CDCl_3$): δ 183.9*, 180.4**, 35.9**, 33.9*, 18.7*, 18.1**, 13.6**.

***n*-butyric acid**

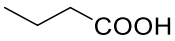

Synthesized following the general procedure for the carbonylation of aliphatic alcohols (Procedure B); No H_2O was used for the reaction. Colorless liquid, combined isolated yield: 38%, 278 mg (1:2, b:l); distinct signals of linear isomer are marked * and those of branched **. Rf = 0.4 (0 to 25% EtOAc in petroleum ether). ^{1}H NMR (301 MHz, $CDCl_3$): δ 11.14 (br s, 3H, overlapping), 2.71 – 2.49** (m, 1H), 2.35* (t, J = 7.4 Hz, 4H), 1.79 – 1.57* (m, 4H), 1.22** (d, J = 7.0 Hz, 6H), 0.99* (t, J = 7.4 Hz, 6H). $^{13}C\{^1H\}$ NMR (76 MHz, CDCl3): δ 183.9**, 180.4*, 35.9*, 33.9**, 18.7**, 18.1*, 13.6*.

S6.3. NMR Spectra of catalytic products

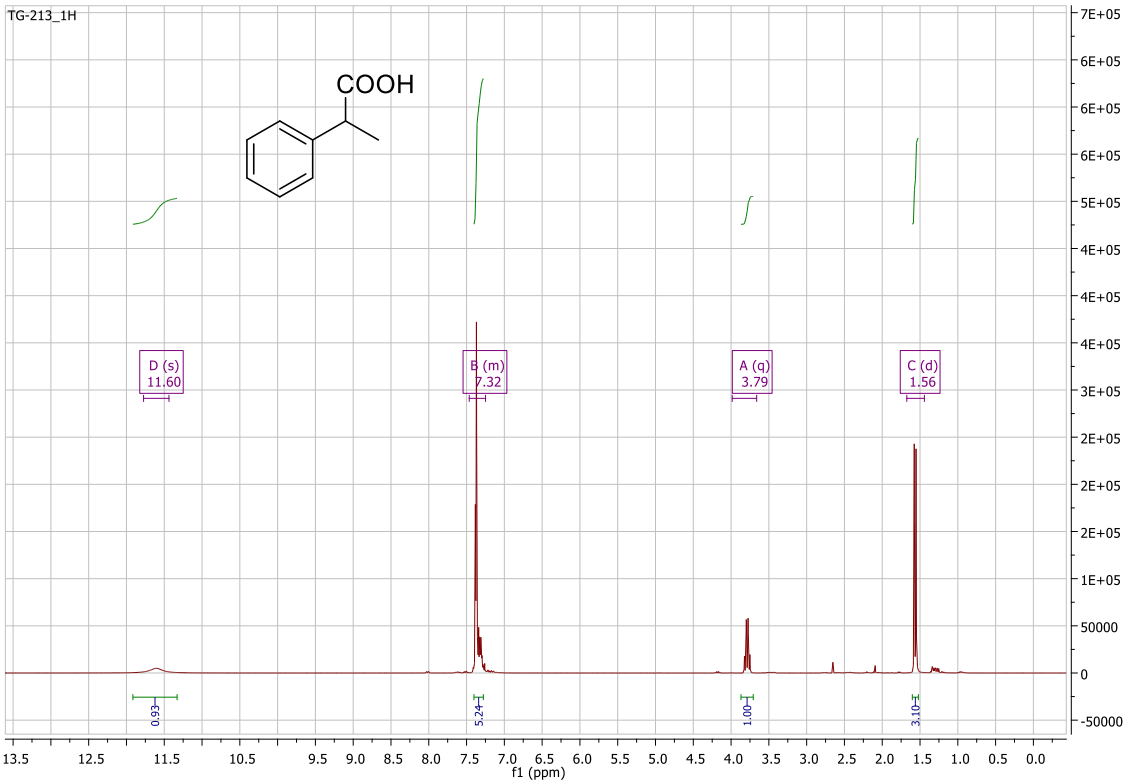

Figure S6. ^{1}H NMR spectrum (300 MHz, $CDCl_3$, 298K)

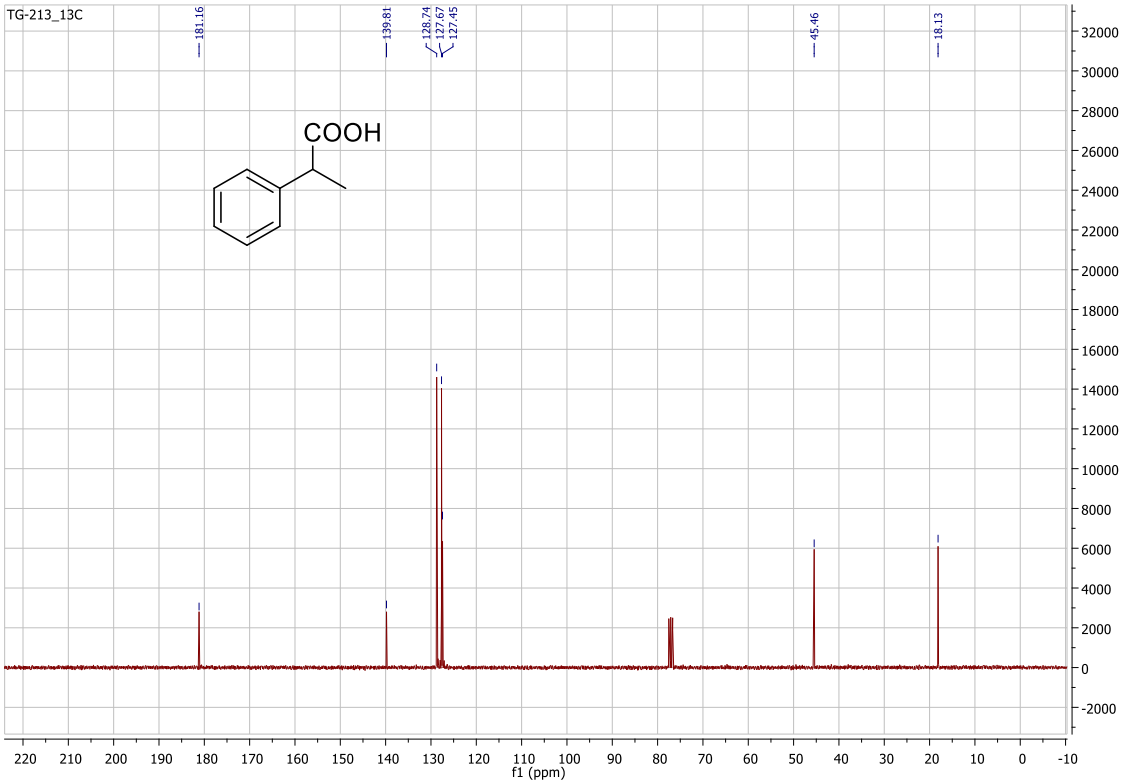

Figure S7. $^{13}C\{^{1}H\}$ NMR spectrum (76 MHz, $CDCl_3$, 298K)

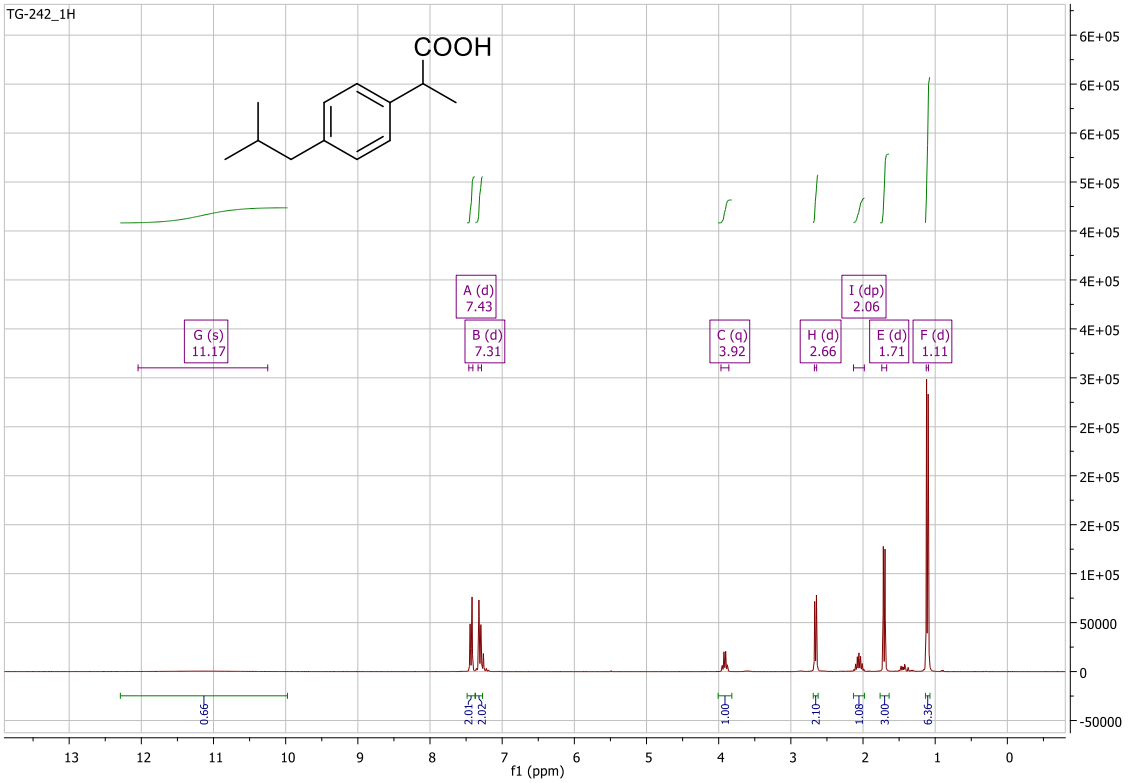

Figure S8. ^{1}H NMR spectrum (300 MHz, $CDCl_3$, 298K)

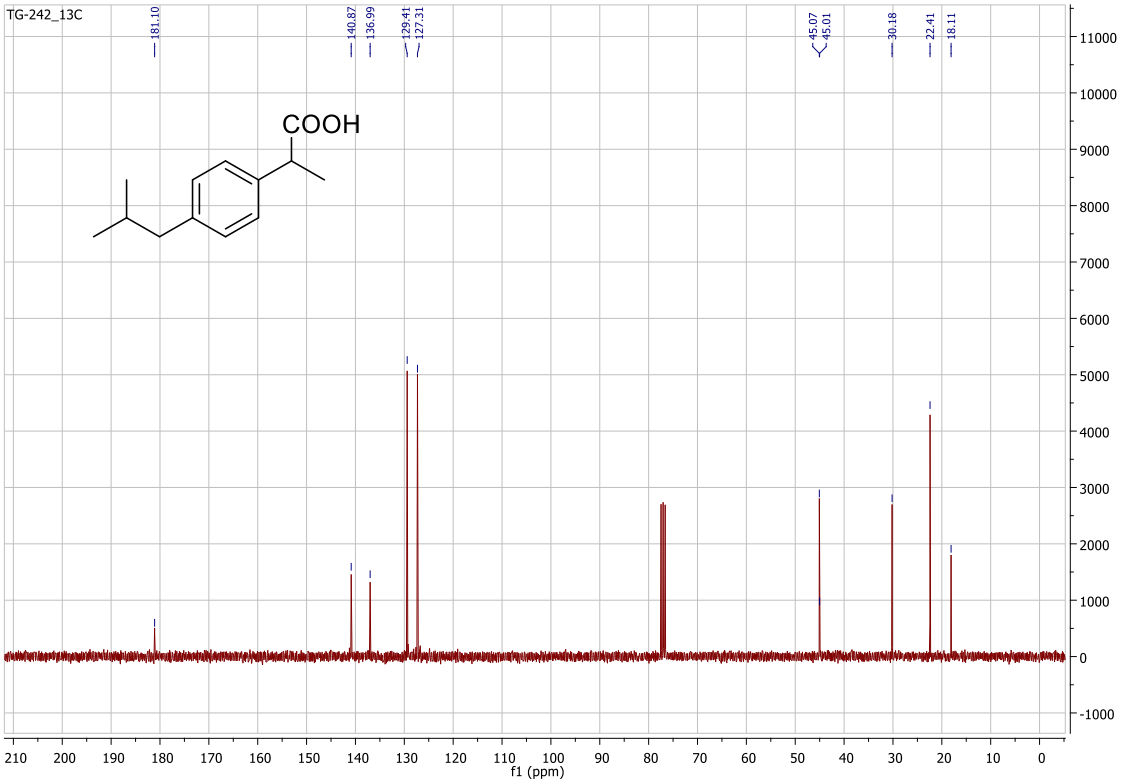

Figure S9. $^{13}C\{^{1}H\}$ NMR spectrum (76 MHz, $CDCl_3$, 298K)

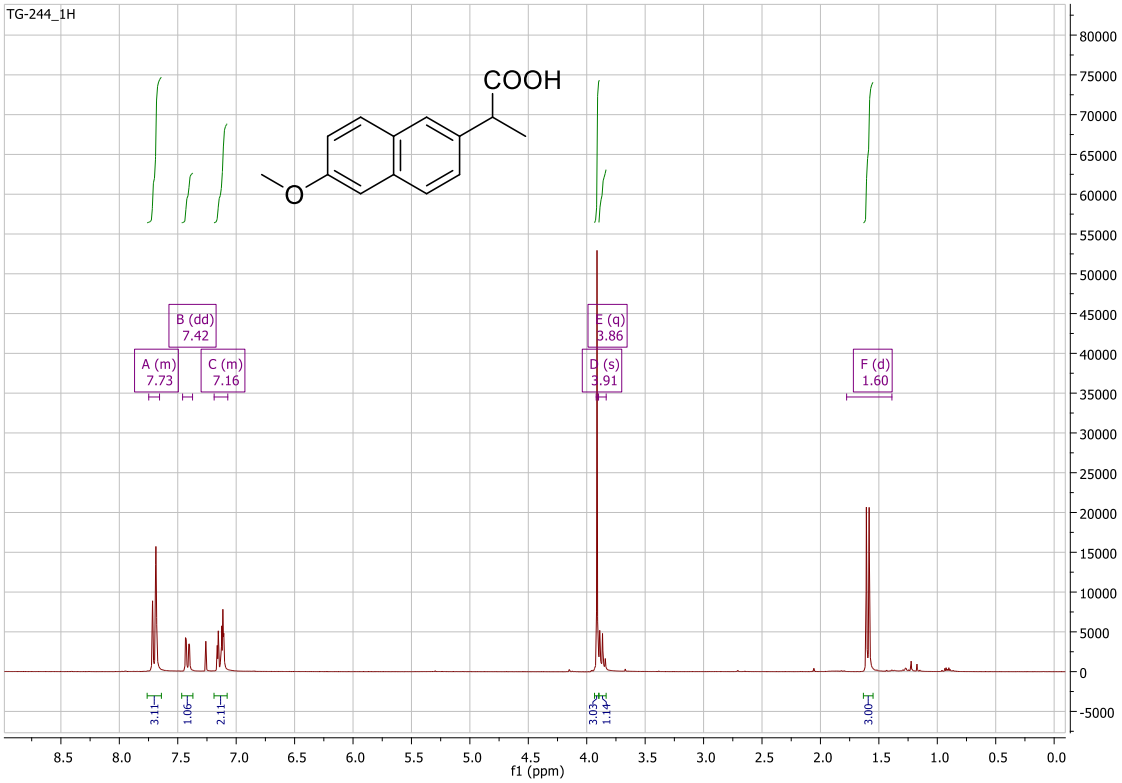

Figure S10. ^{1}H NMR spectrum (300 MHz, $CDCl_3$, 298K)

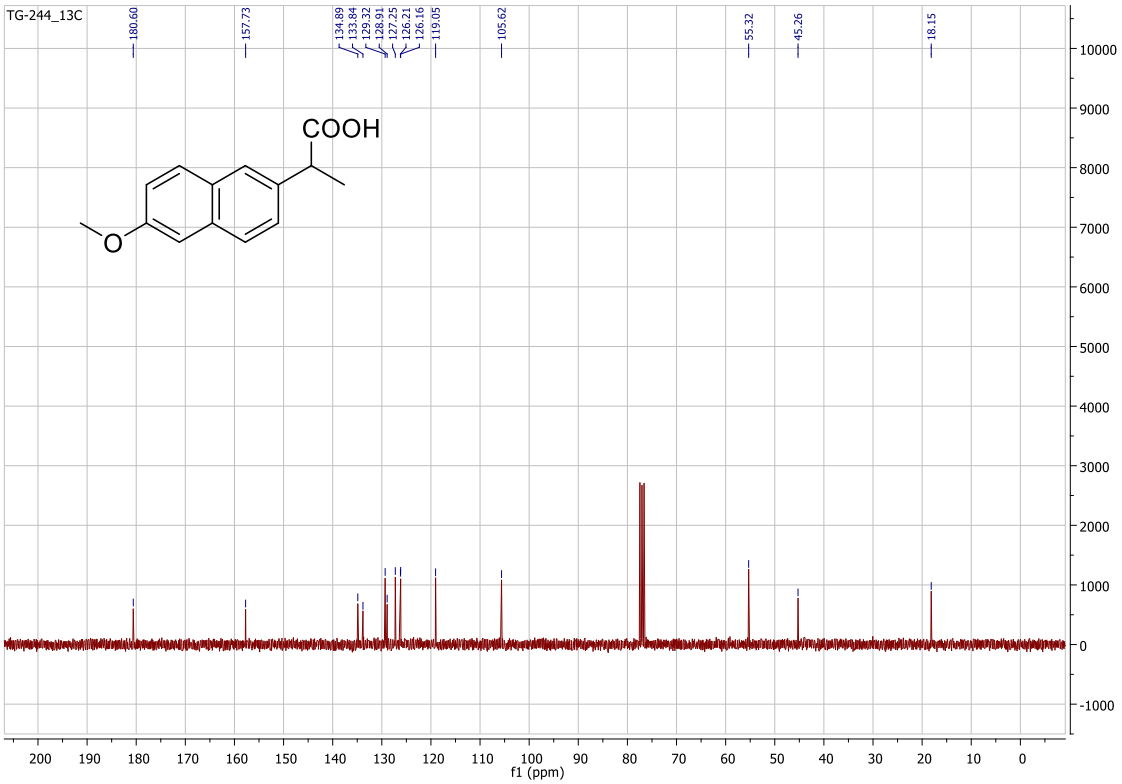

Figure S11. $^{13}C\{^{1}H\}$ NMR spectrum (76 MHz, $CDCl_3$, 298K)

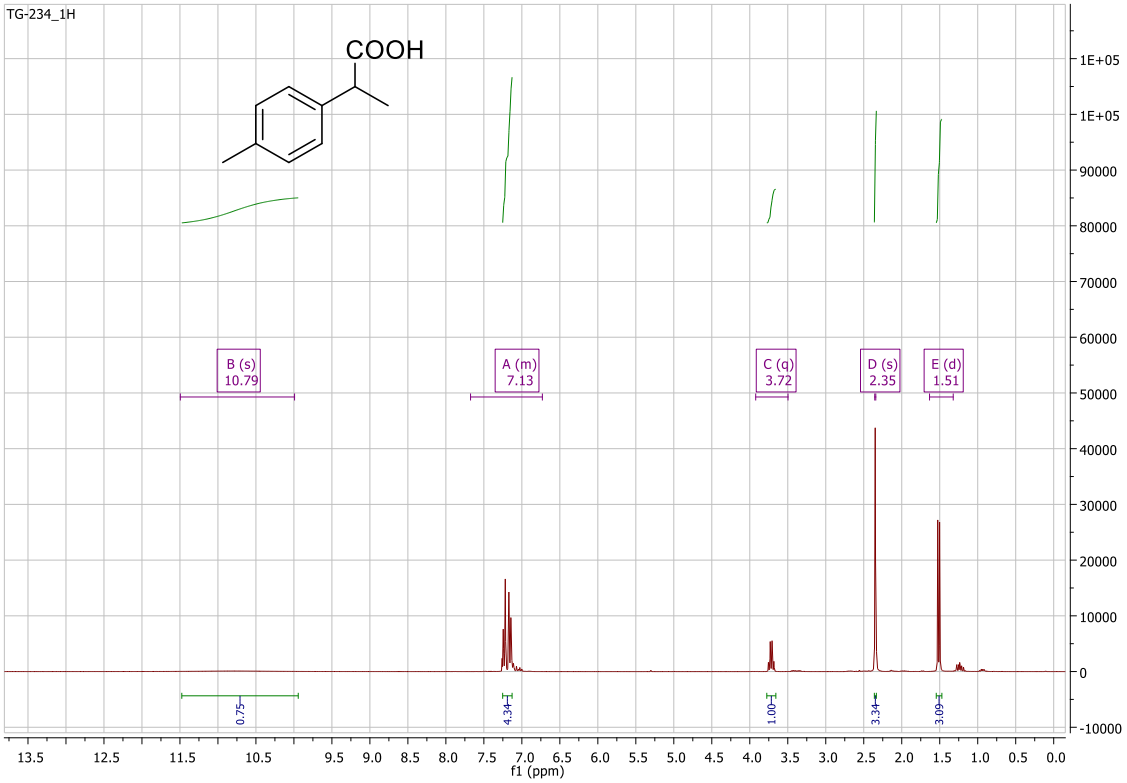

Figure S12. ^{1}H NMR spectrum (300 MHz, $CDCl_3$, 298K)

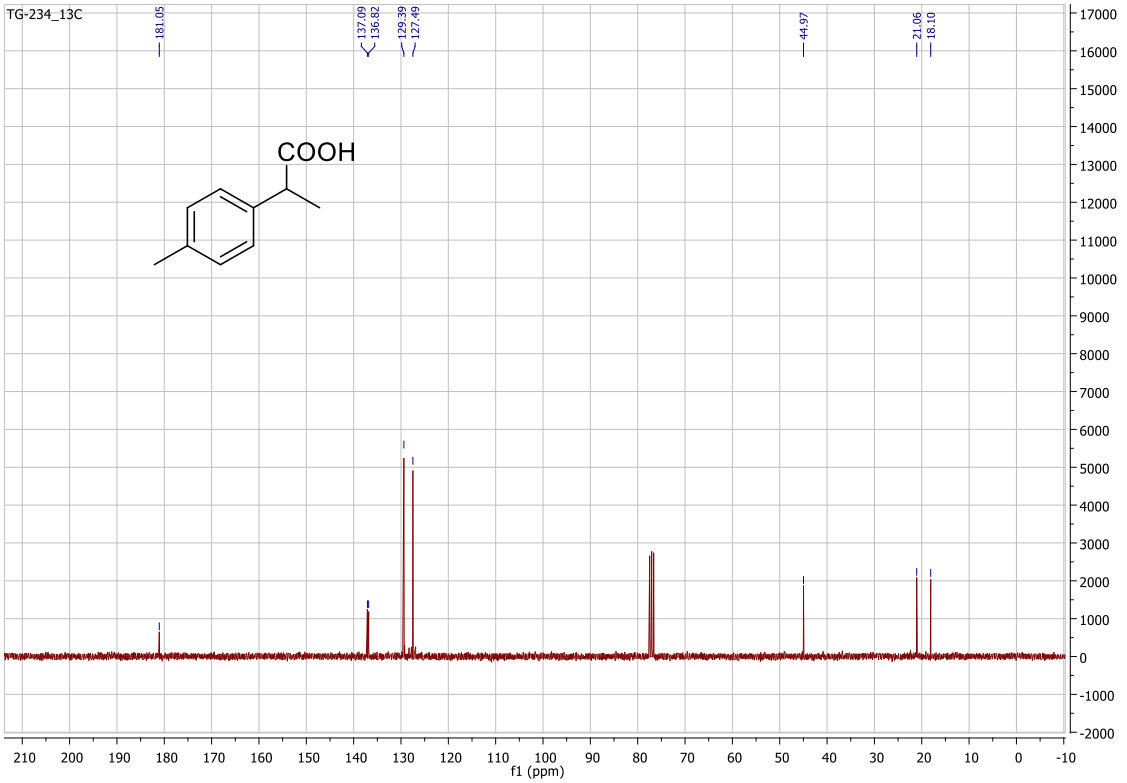

Figure S13. $^{13}C\{^{1}H\}$ NMR spectrum (76 MHz, $CDCl_3$, 298K)

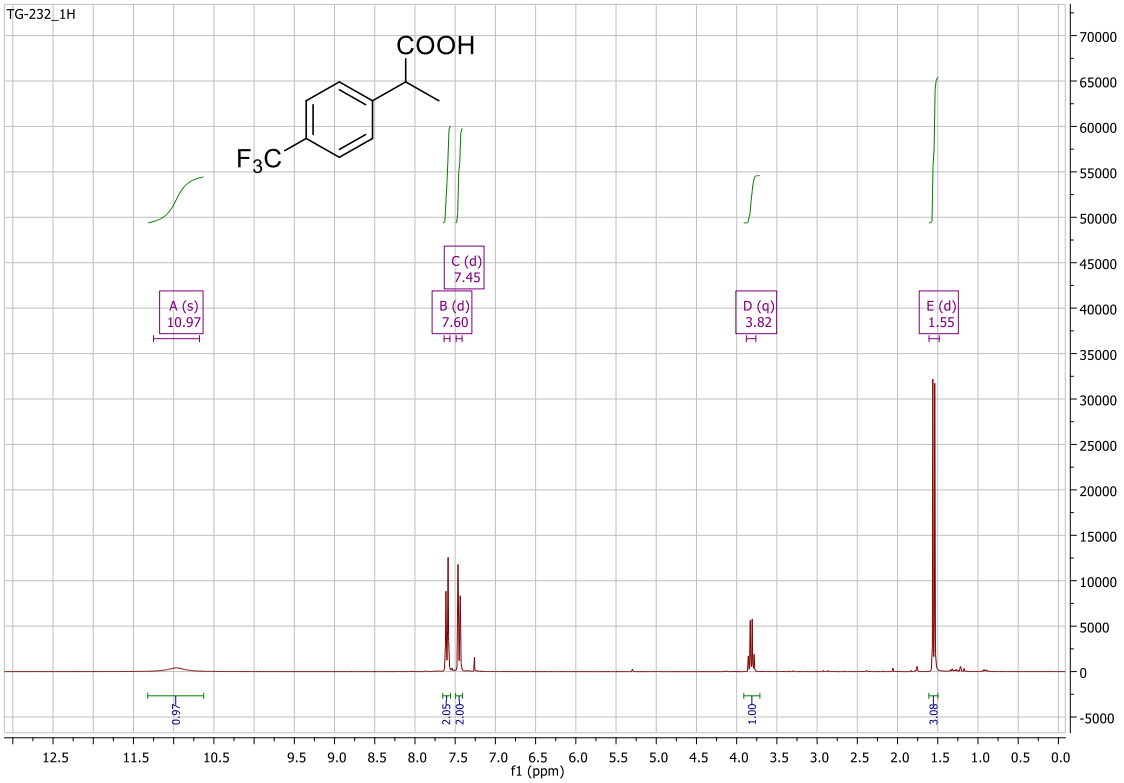

Figure S14. ^{1}H NMR spectrum (300 MHz, $CDCl_3$, 298K)

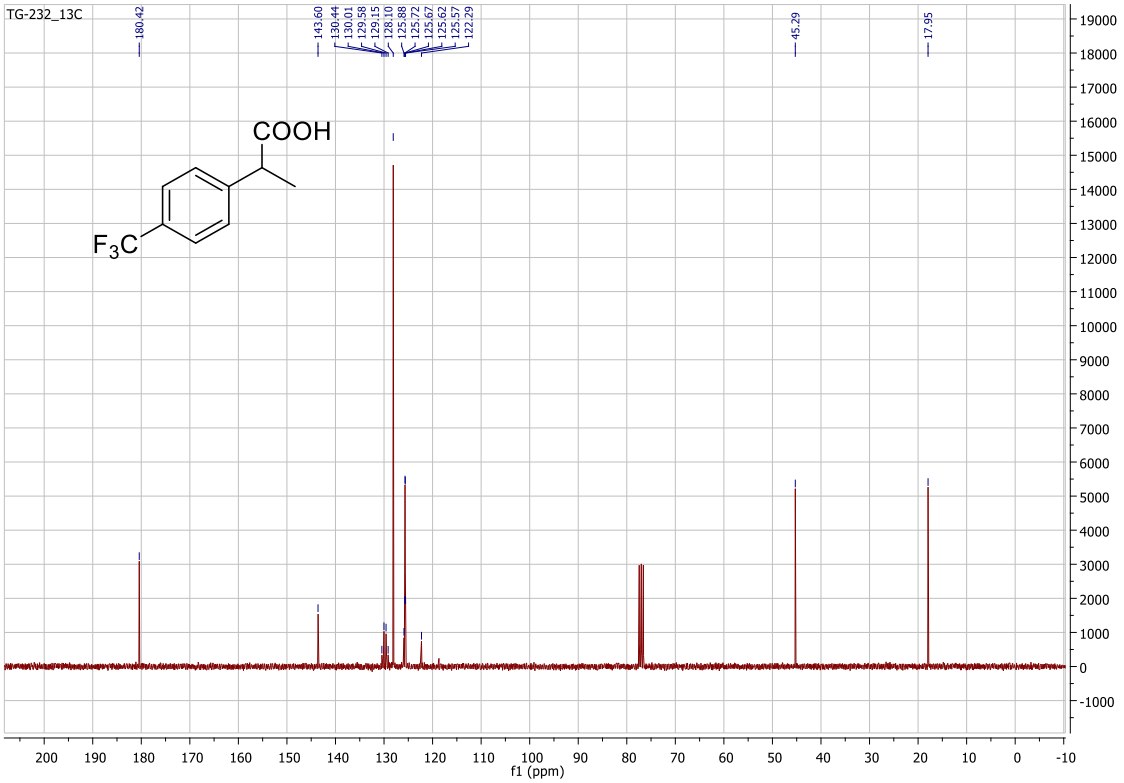

Figure S15. $^{13}C\{^{1}H\}$ NMR spectrum (76 MHz, $CDCl_3$, 298K)

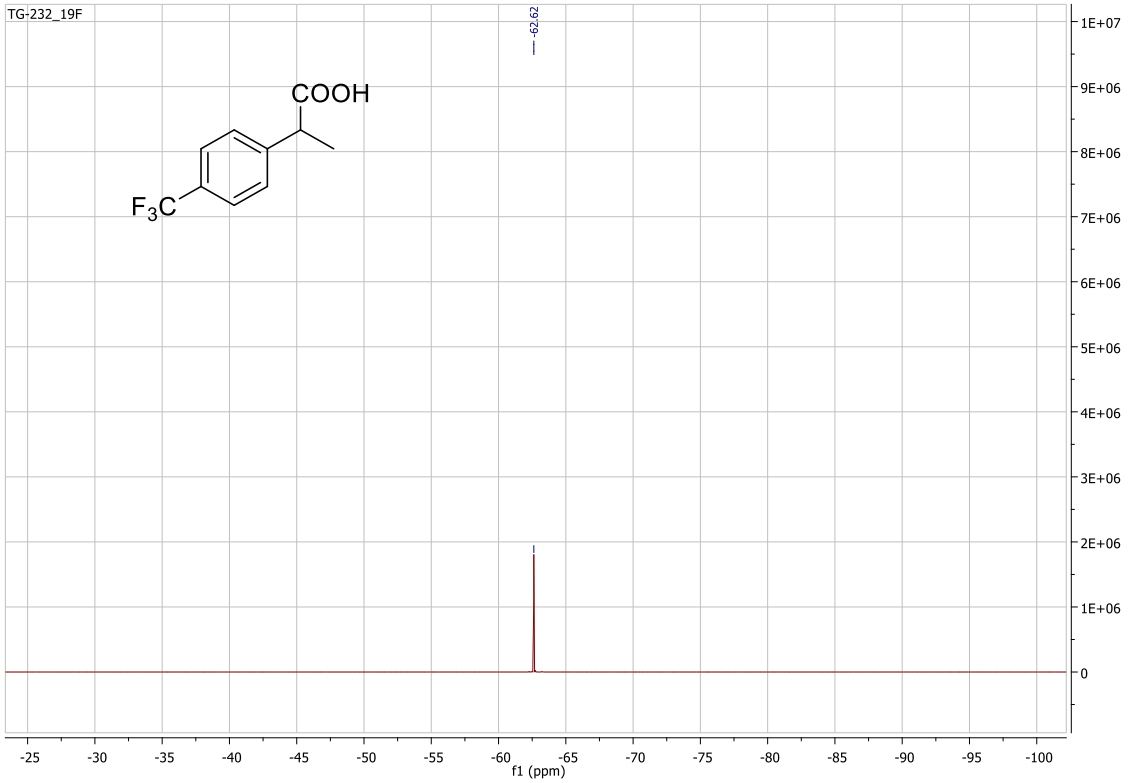

Figure S16. ^{19}F NMR spectrum (300 MHz, $CDCl_3$, 298K)

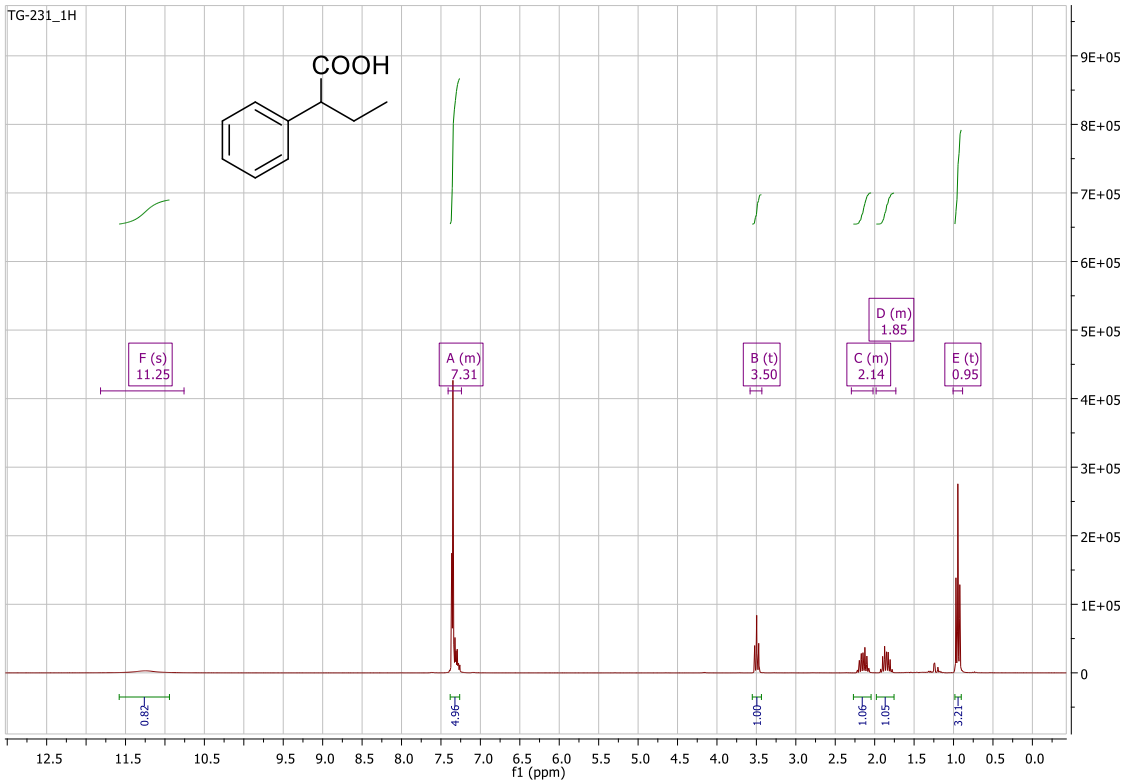

Figure S17. ^{1}H NMR spectrum (300 MHz, $CDCl_3$, 298K)

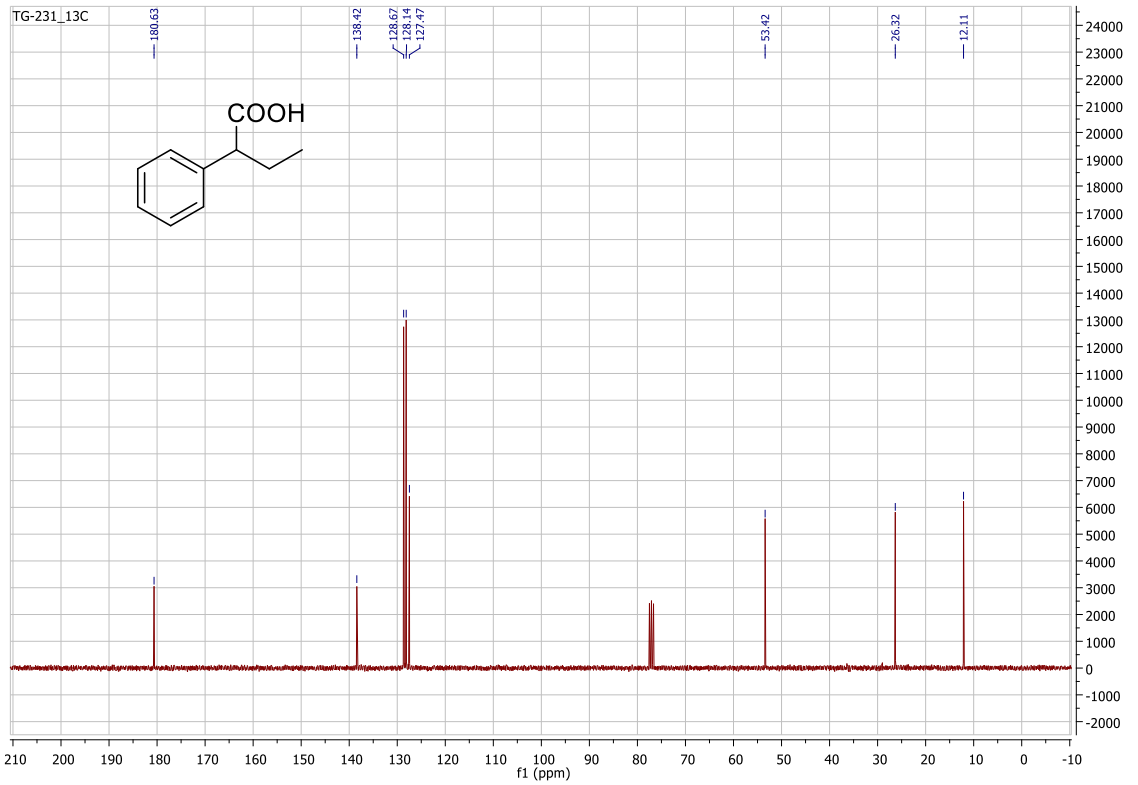

Figure S18. $^{13}C\{^{1}H\}$ NMR spectrum (76 MHz, $CDCl_3$, 298K)

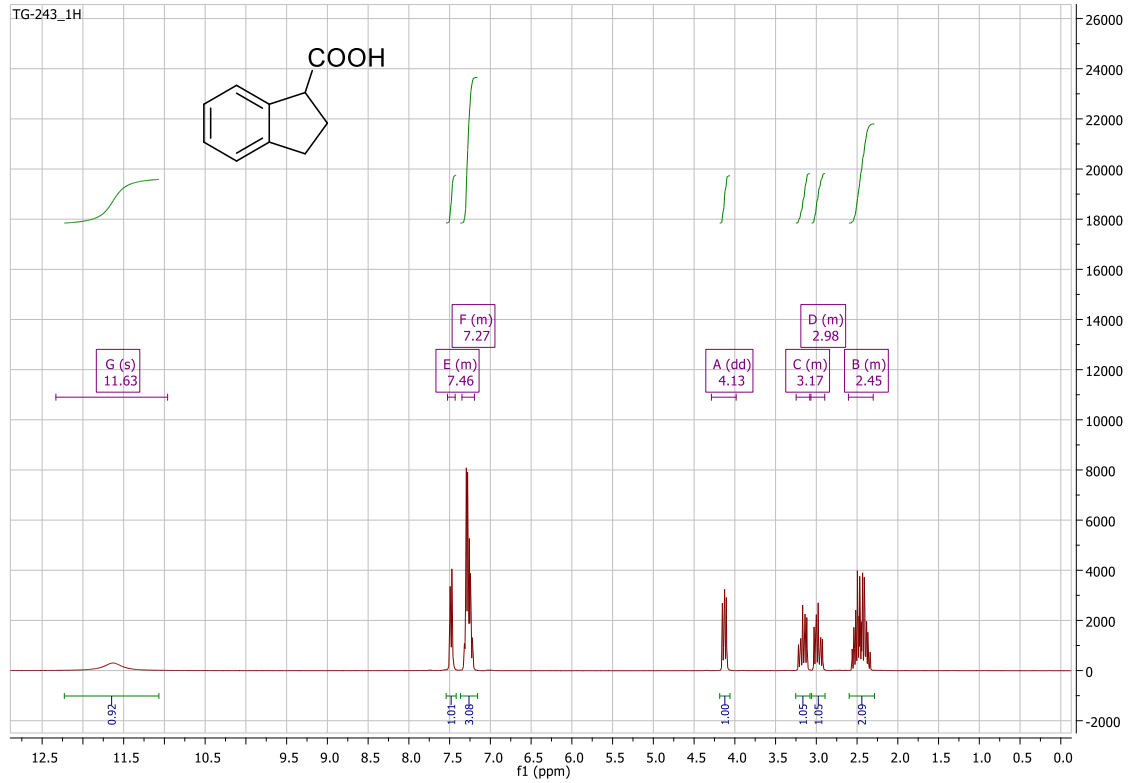

Figure S19. ^{1}H NMR spectrum (300 MHz, $CDCl_3$, 298K)

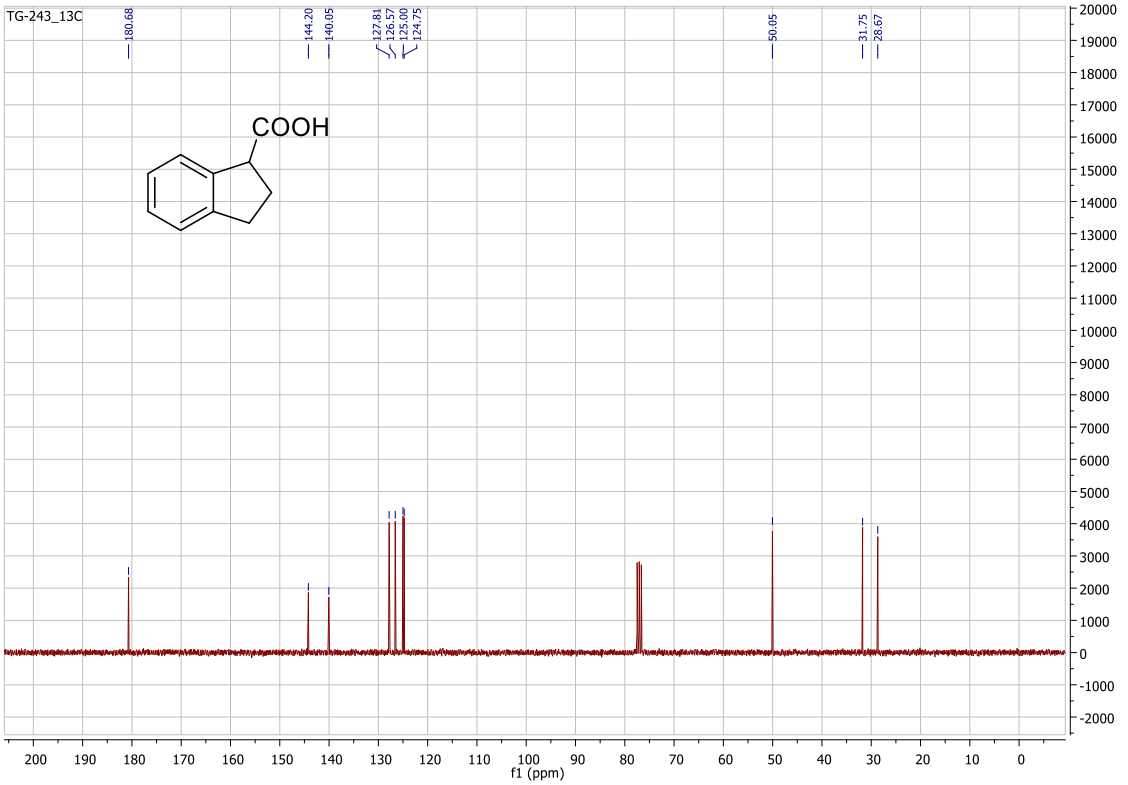

Figure S20. $^{13}C\{^{1}H\}$ NMR spectrum (76 MHz, $CDCl_3$, 298K)

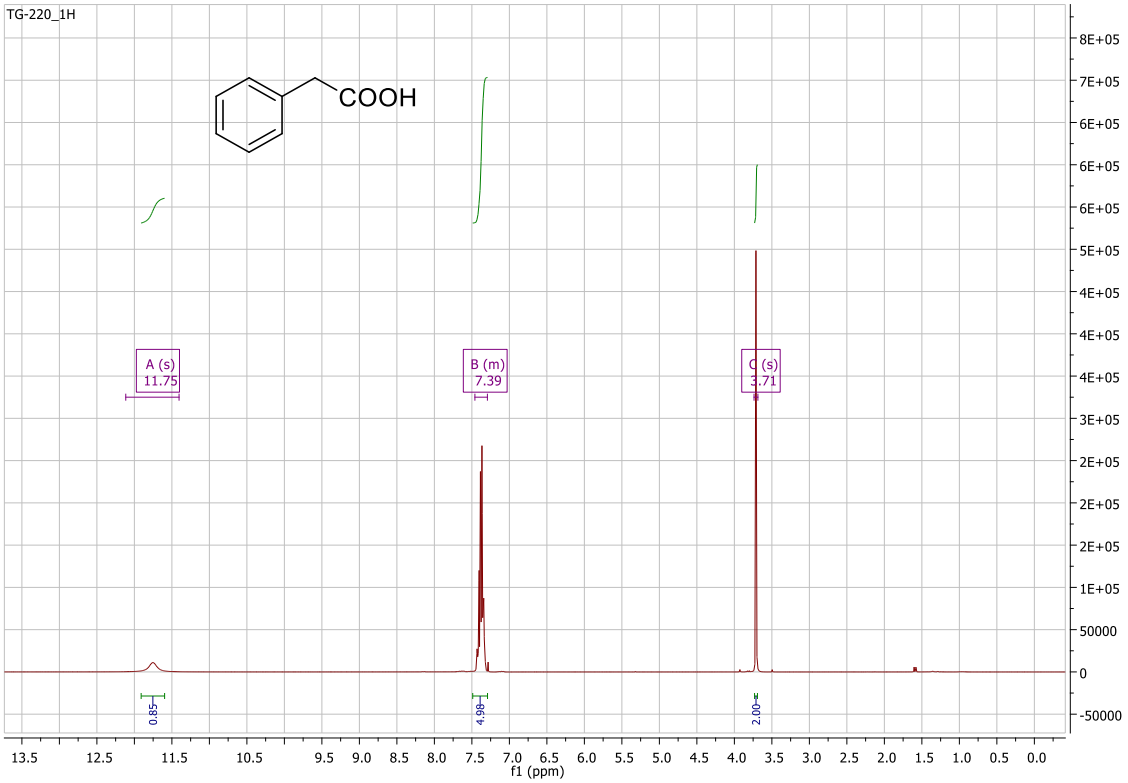

Figure S21. ^{1}H NMR spectrum (300 MHz, $CDCl_3$, 298K)

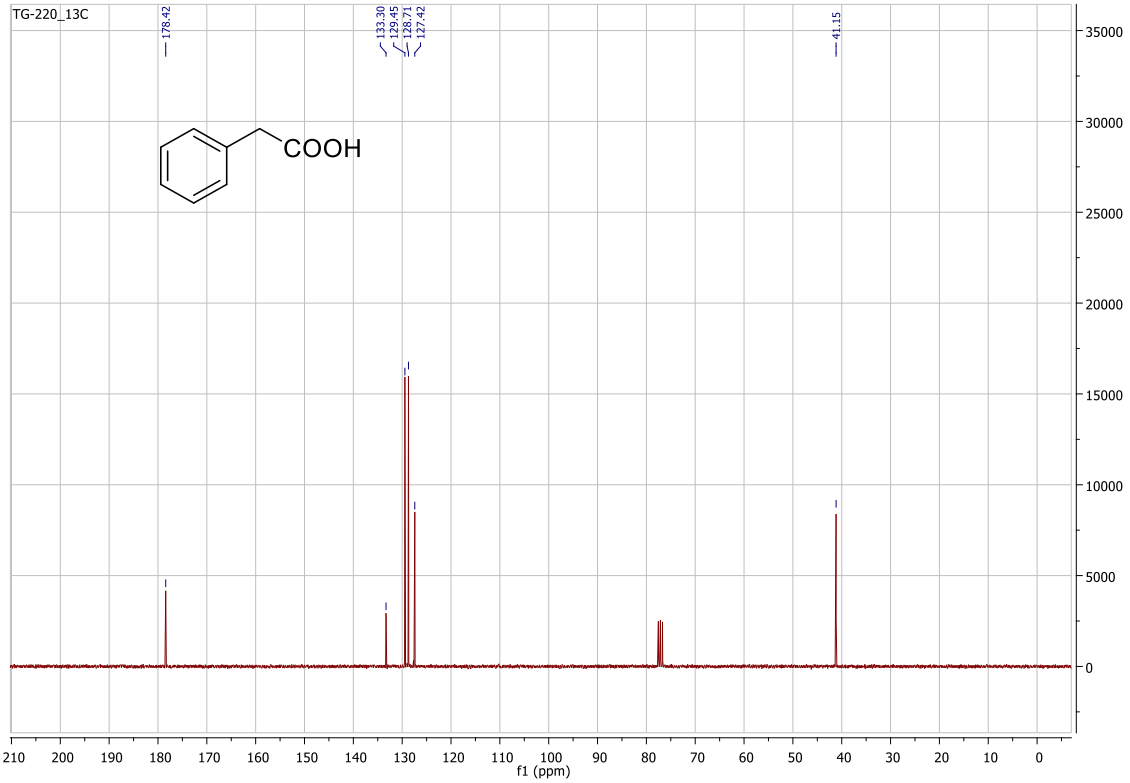

Figure S22. $^{13}C\{^{1}H\}$ NMR spectrum (76 MHz, $CDCl_3$, 298K)

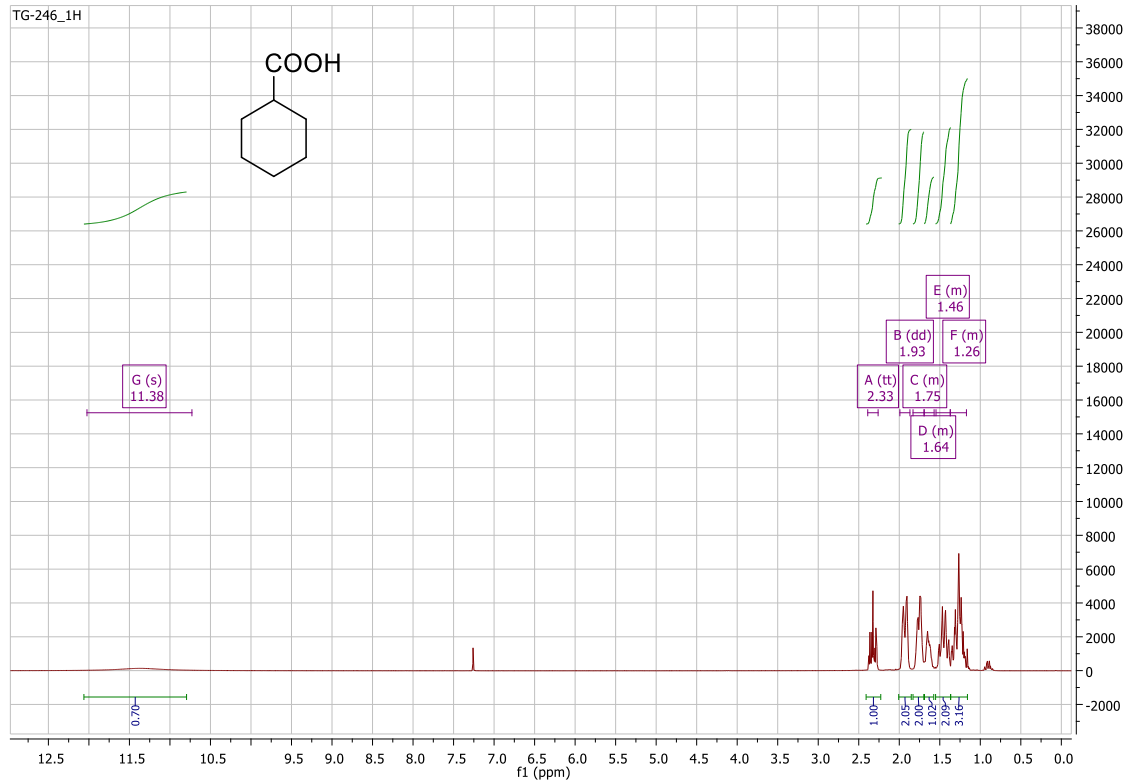

Figure S23. ^{1}H NMR spectrum (300 MHz, $CDCl_3$, 298K)

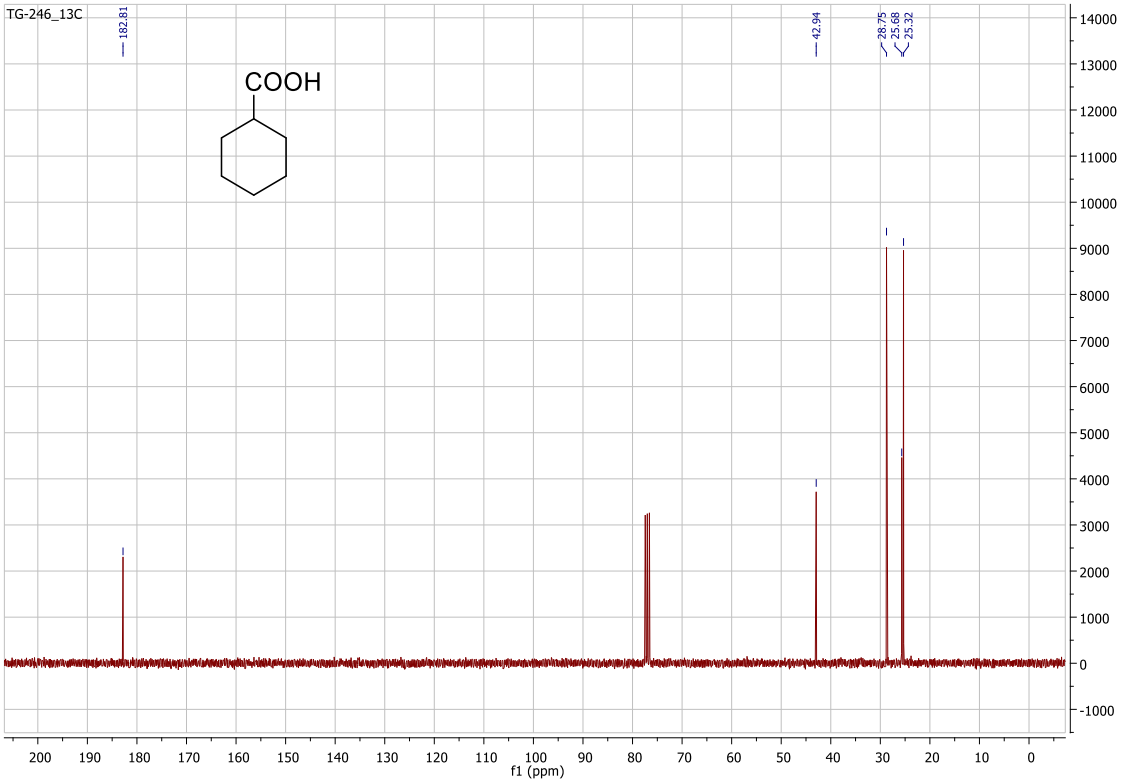

Figure S24. $^{13}C\{^{1}H\}$ NMR spectrum (76 MHz, $CDCl_3$, 298K)

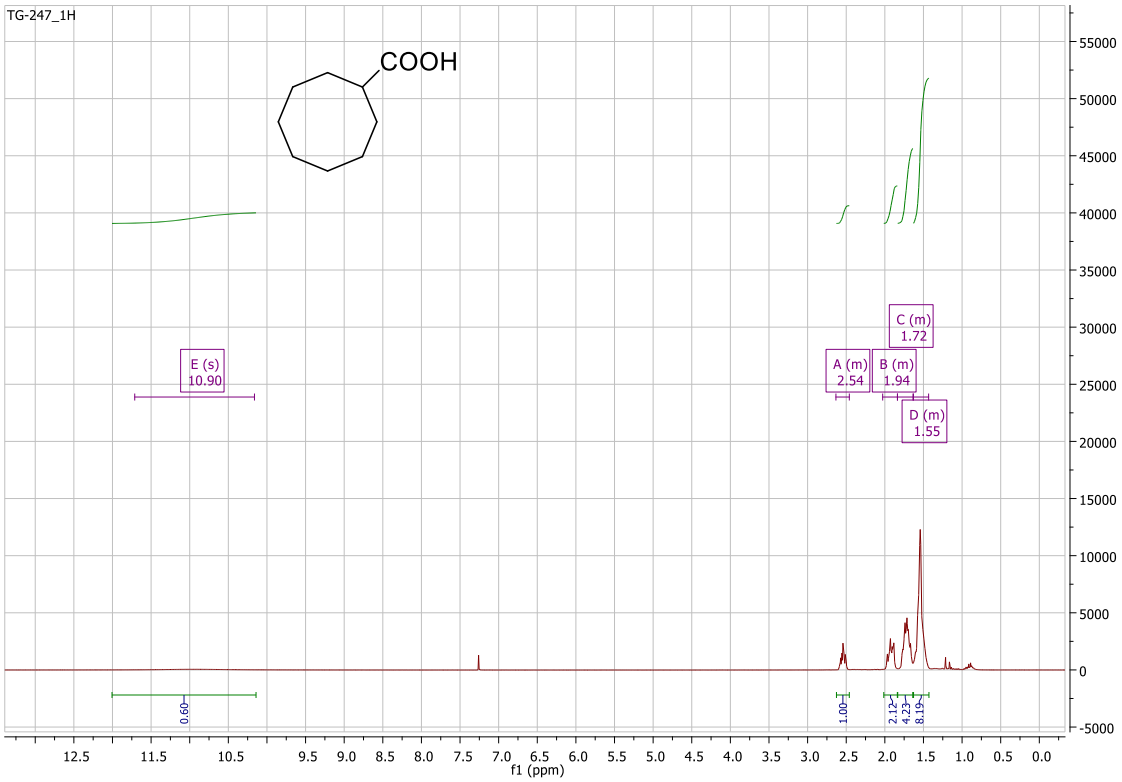

Figure S25. ^{1}H NMR spectrum (300 MHz, $CDCl_3$, 298K)

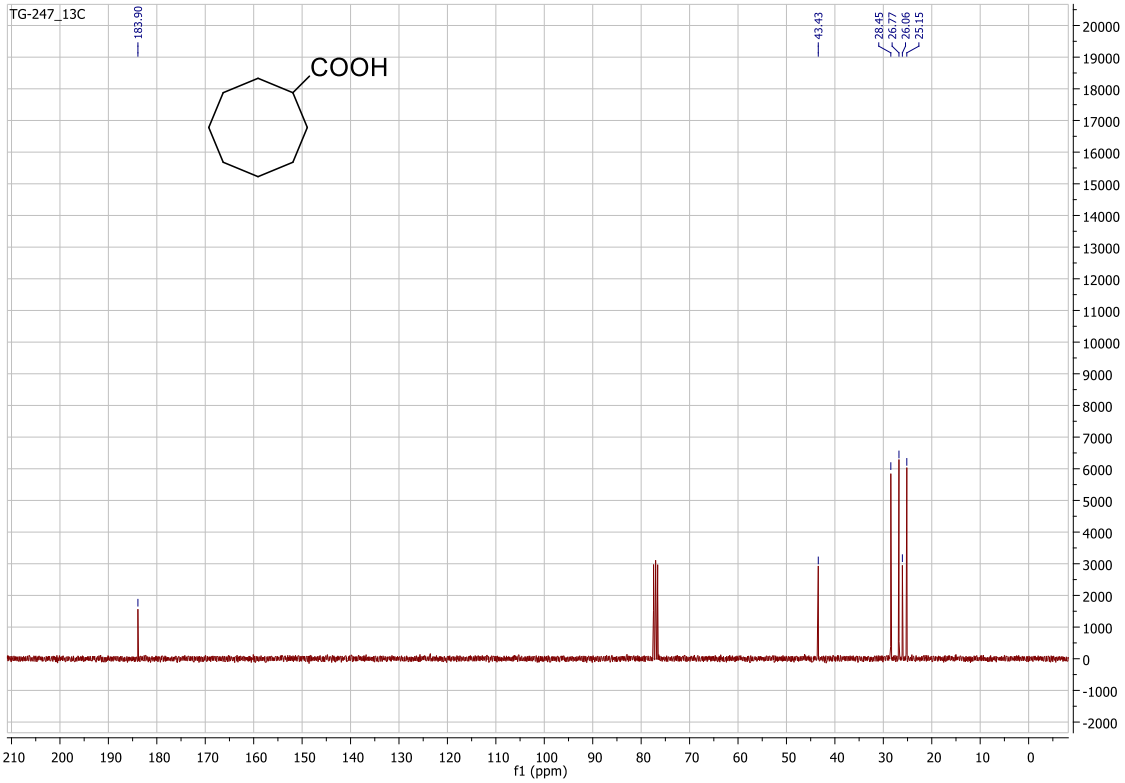

Figure S26. $^{13}C\{^{1}H\}$ NMR spectrum (76 MHz, $CDCl_3$, 298K)

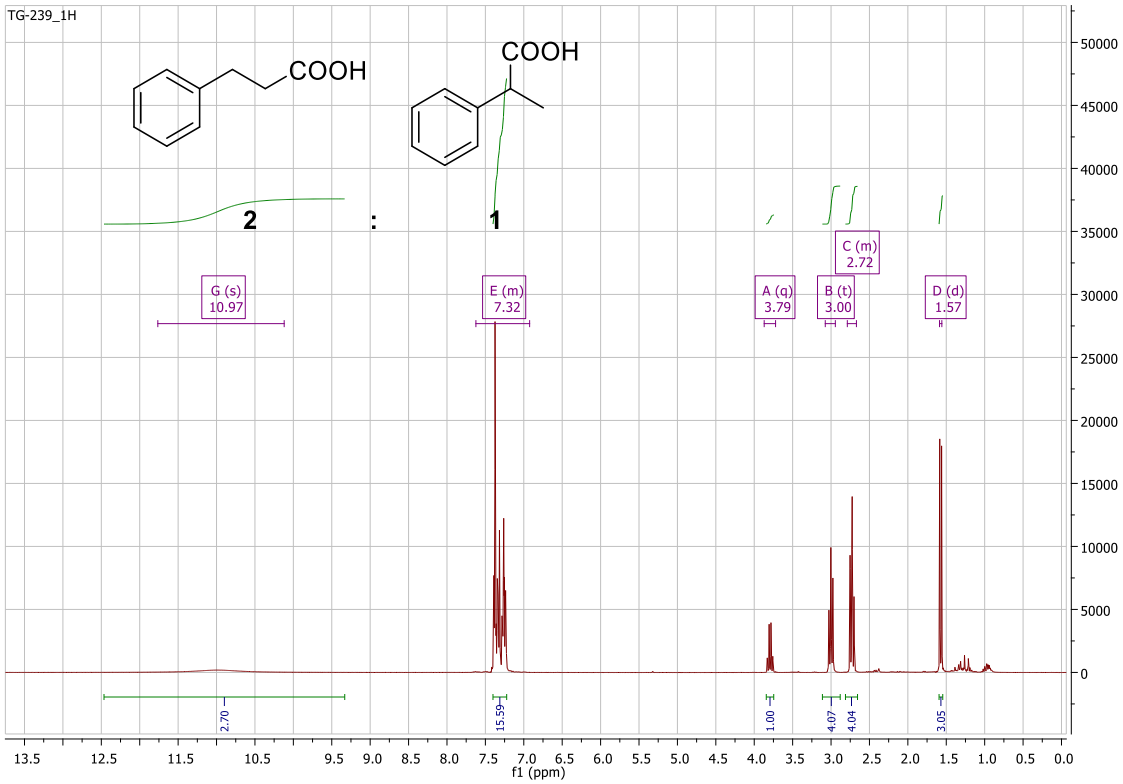

Figure S27. ^{1}H NMR spectrum (300 MHz, $CDCl_3$, 298K)

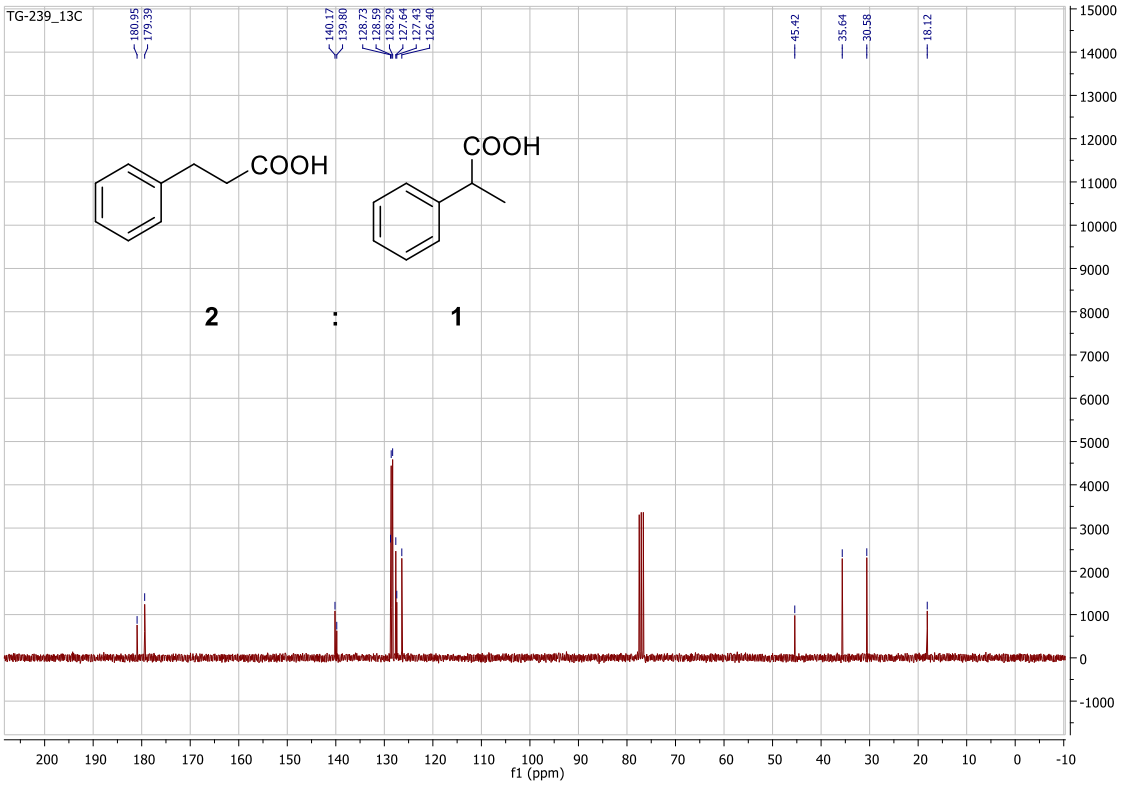

Figure S28. $^{13}C\{^{1}H\}$ NMR spectrum (76 MHz, $CDCl_3$, 298K)

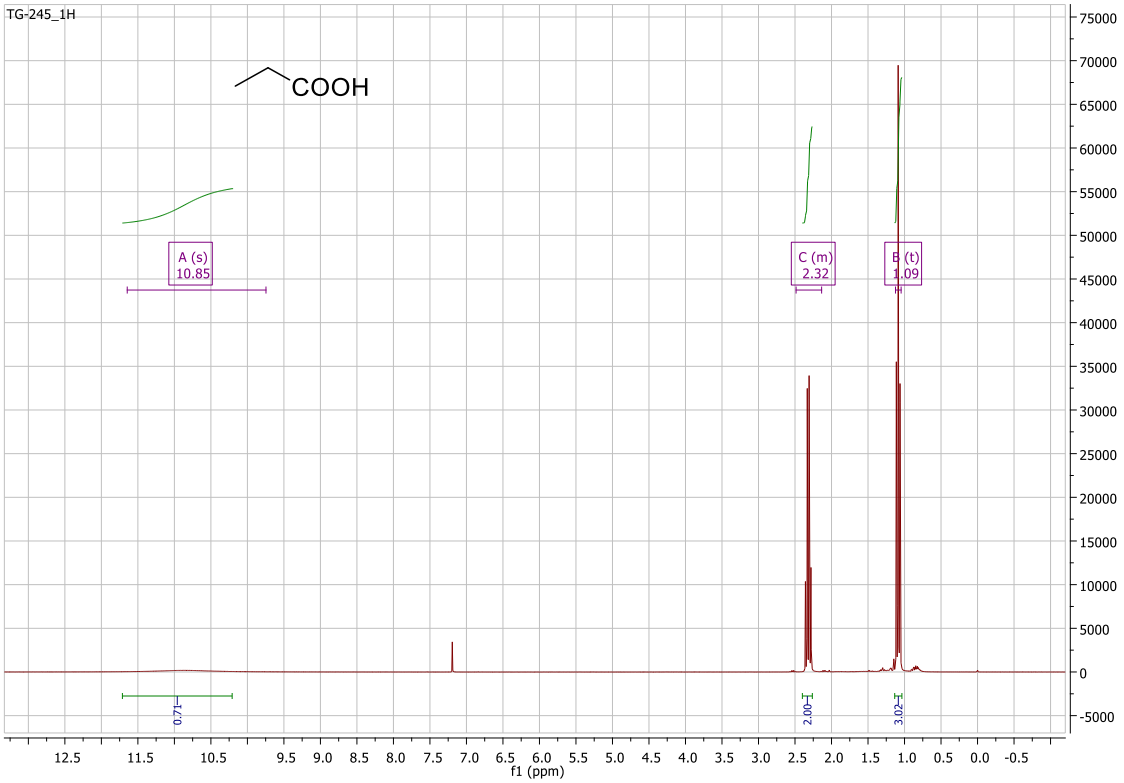

Figure S29. ^{1}H NMR spectrum (300 MHz, $CDCl_3$, 298K)

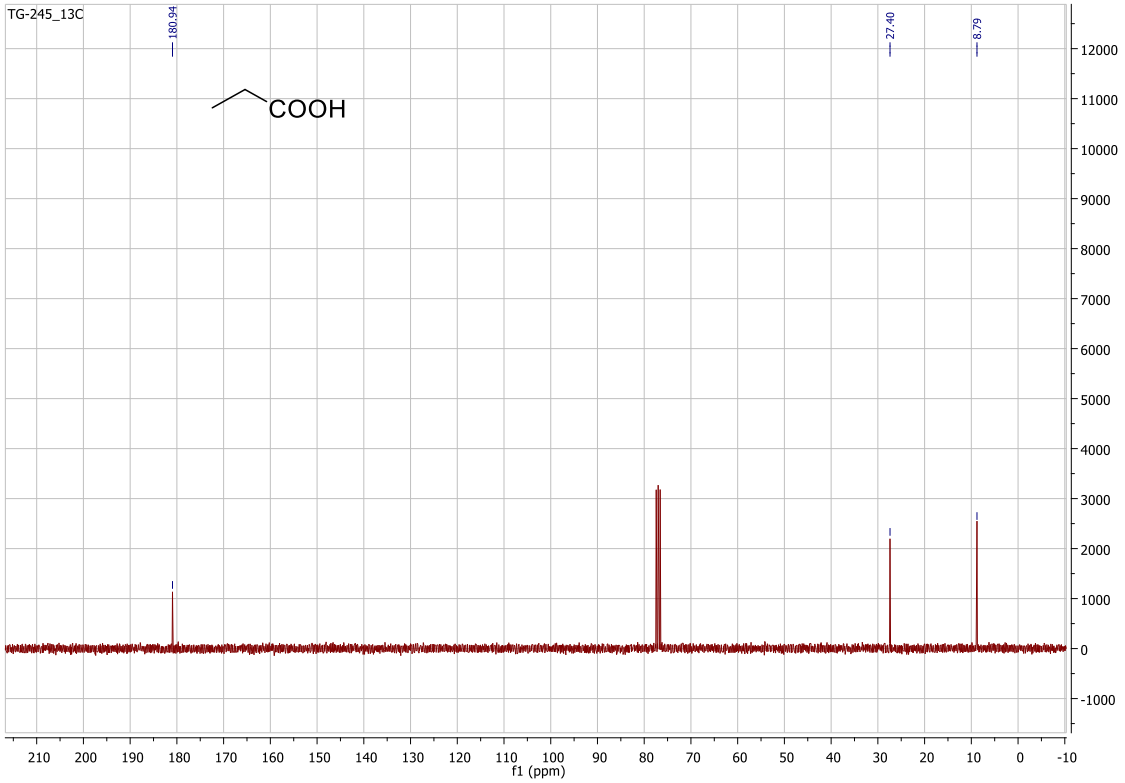

Figure S30. $^{13}C\{^{1}H\}$ NMR spectrum (76 MHz, $CDCl_3$, 298K)

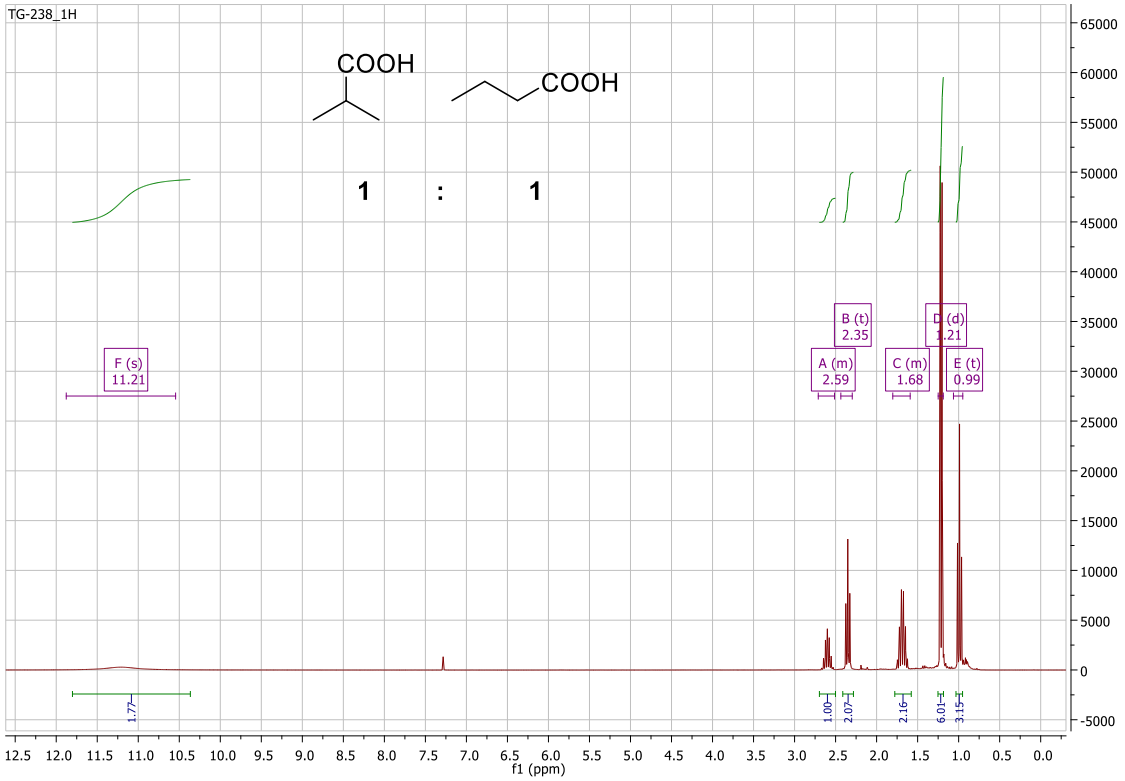

Figure S31. ^{1}H NMR spectrum (300 MHz, $CDCl_3$, 298K)

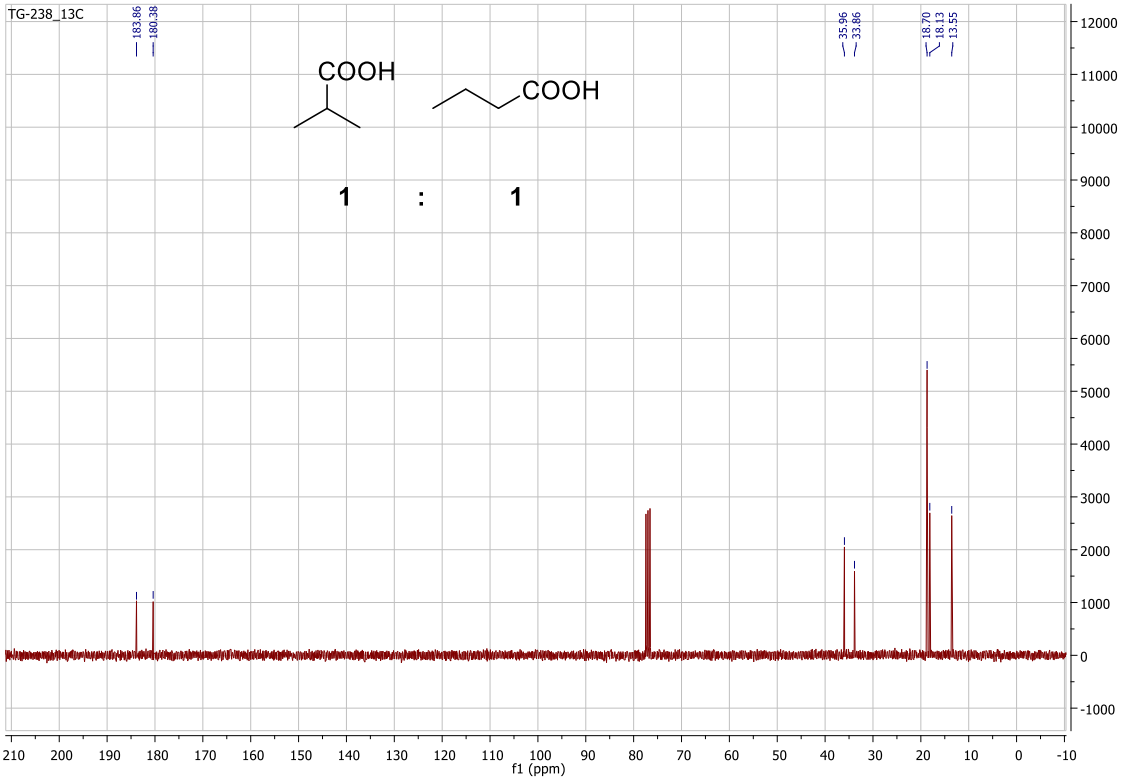

Figure S32. $^{13}C\{^{1}H\}$ NMR spectrum (76 MHz, $CDCl_3$, 298K)

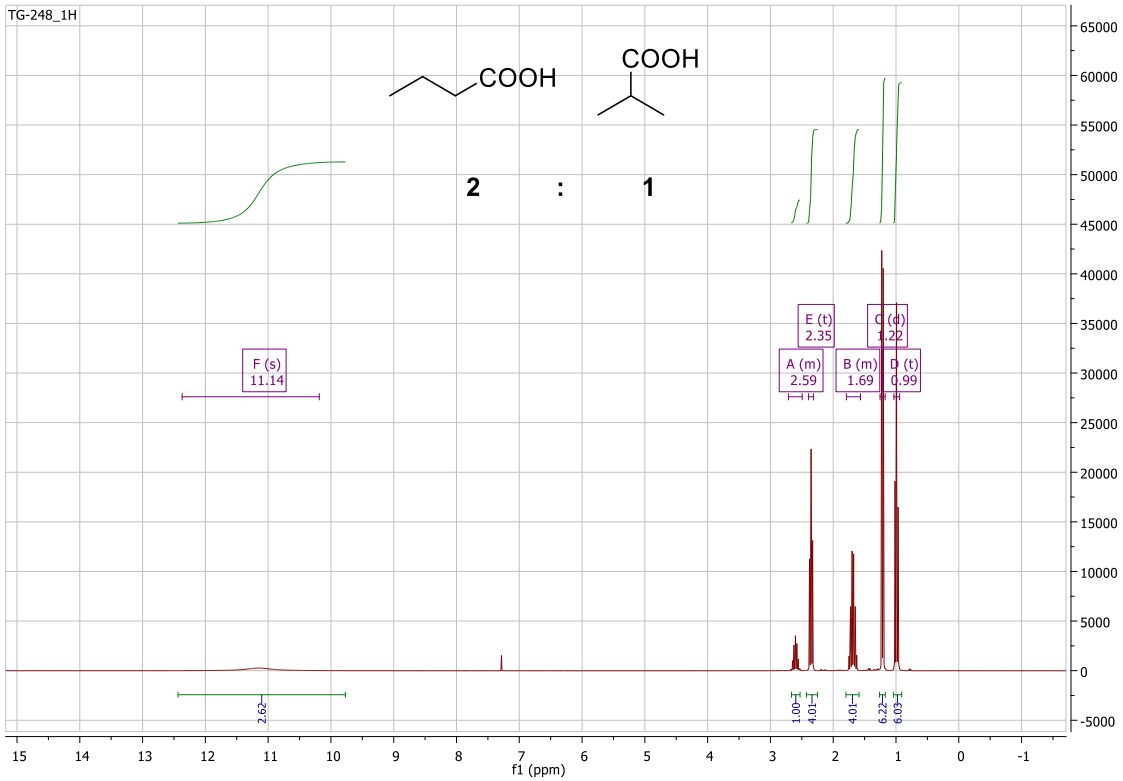

Figure S33. ^{1}H NMR spectrum (300 MHz, $CDCl_3$, 298K)

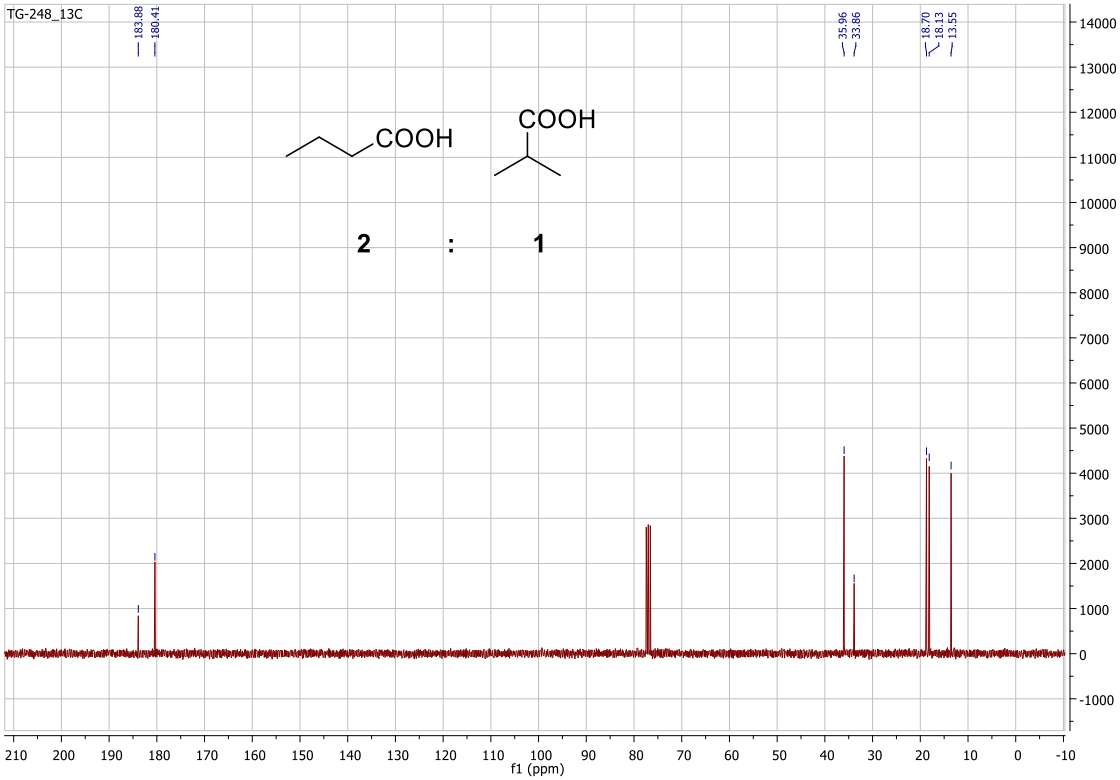

Figure S34. $^{13}C\{^{1}H\}$ NMR spectrum (76 MHz, $CDCl_3$, 298K)

S7. XYZ coordinates of the computed structures

The supplemental file coordinates.xyz contains the computed Cartesian coordinates of all of the molecules reported in this study. The file may be opened as a text file to read the coordinates, or opened directly by a molecular modeling program such as Mercury (version 3.3 or later, http://www.ccdc.cam.ac.uk/pages/Home.aspx) for visualization and analysis.